Circulation Research
JOURNAL OF THE AMERICAN HEART ASSOCIATION

Proteomic and Metabolomic Analysis of Smooth Muscle Cells Derived From the Arterial Media and Adventitial Progenitors of Apolipoprotein E –Deficient Mice

Manuel Mayr, Anna Zampetaki, Anissa Sidibe, Ursula Mayr, Xiaoke Yin, Ayesha I. De Souza, Yuen-Li Chung, Basetti Madhu, Paul H. Quax, Yanhua Hu, John R. Griffiths and Qingbo Xu

Circ Res. 2008;102:1046-1056; originally published online April 3, 2008;
doi: 10.1161/CIRCRESAHA.108.174623
Circulation Research is published by the American Heart Association, 7272 Greenville Avenue, Dallas, TX 75231

Print ISSN: 0009-7330. Online ISSN: 1524-4571

Proteomic and Metabolomic Analysis of Smooth Muscle Cells Derived From the Arterial Media and Adventitial Progenitors of Apolipoprotein E–Deficient Mice

Manuel Mayr, Anna Zampetaki, Anissa Sidibe, Ursula Mayr, Xiaoke Yin, Ayesha I. De Souza, Yuen-Li Chung, Basetti Madhu, Paul H. Quax, Yanhua Hu, John R. Griffiths, Qingbo Xu

Abstract—We have recently demonstrated that stem cell antigen 1–positive (Sca-1$^+$) progenitors exist in the vascular adventitia of apolipoprotein E–deficient (apoE$^{-/-}$) mice and contribute to smooth muscle cell (SMC) accumulation in vein graft atherosclerosis. Using a combined proteomic and metabolomic approach, we now characterize these local progenitors, which participate in the formation of native atherosclerotic lesions in chow-fed apoE$^{-/-}$ mice. Unlike Sca-1$^+$ progenitors from embryonic stem cells, the resident Sca-1$^+$ stem cell population from the vasculature acquired a mature aortic SMC phenotype after platelet-derived growth factor-BB stimulation. It shared proteomic and metabolomic characteristics of apoE$^{-/-}$ SMCs, which were clearly distinct from wild-type SMCs under normoxic and hypoxic conditions. Among the differentially expressed proteins were key enzymes in glucose metabolism, resulting in faster glucose consumption and a compensatory reduction in baseline interleukin-6 secretion. The latter was associated with a marked upregulation of insulin-like growth factor binding proteins (IGFBPs) 3 and 6. Notably, reconstitution of interleukin-6 to levels measured in the conditioned medium of wild-type SMCs attenuated the elevated IGFBP expression in apoE$^{-/-}$ SMCs and their vascular progenitors. This coregulation of apoE, interleukin-6, and IGFBPs was replicated in wild-type SMCs from hypercholesterolemic mice and confirmed by silencing apoE expression in SMCs from normocholesterolemic mice. In summary, we provide evidence that Sca-1$^+$ progenitors contribute to native atherosclerosis in apoE$^{-/-}$ mice, that apoE deficiency and hypercholesterolemia alter progenitor cell behavior, and that inflammatory cytokines such as interleukin-6 act as metabolic regulators in SMCs of hyperlipidemic mice. **(*Circ Res*. 2008;102:1046-1056.)**

Key Words: atherosclerosis ■ insulin-like growth factor-1 ■ progenitor cells ■ proteomics ■ vascular smooth muscle

With the introduction of apolipoprotein (apo)E-deficient strains, the mouse became the preferred animal model in cardiovascular research.[1] ApoE is a glycoprotein that is synthesized in the liver and the brain, but it is also produced locally in the vessel wall, mainly in infiltrating monocytes and macrophages,[2] and gets recruited from the circulation after vascular injury.[3] Besides apoE-mediated cholesterol transport, lipid-independent effects of apoE also have relevance in vitro and in vivo. For instance, apoE is synthesized in quiescent but not actively proliferating smooth muscle cells (SMCs) in culture[4] and suppresses growth factor and oxidized LDL–induced SMC migration and proliferation.[5] A possible role of apoE in modulation of SMC growth in vivo is supported by observations that the numbers of intimal SMCs are increased in fibroproliferative atherosclerotic plaques of chow-fed apoE$^{-/-}$ mice but reduced after vascular injury in transgenic mice overexpressing apoE.[1,6] Similarly, we found that vein grafts of apoE$^{-/-}$ mice showed increased neointima formation even if grafted to normolipidemic wild-type animals.[7] Notably, atherosclerosis is more severe in chow-fed apoE$^{-/-}$ mice than in cholesterol-fed apoE$^{+/+}$ mice despite similar plasma cholesterol levels.[8] Differences in protein expression and metabolism between apoE$^{-/-}$ and apoE$^{+/+}$ SMCs, however, remain to be elucidated.

Besides local SMCs, vascular progenitors may contribute to SMC accumulation in vascular disease.[9–14] We focused on a resident population of stem cell antigen 1 positive (Sca-1$^+$) progenitors present in the adventitia of apoE$^{-/-}$ mice that repopulates vein grafts following SMC death.[13,15–17] Although these progenitors express SMC markers on platelet-derived growth factor (PDGF)-BB stimulation,[13] a more comprehensive assessment at the molecular level is needed to establish whether these progenitor cell–derived cells truly belong to the SMC lineage. We have recently used proteom-

Original received May 14, 2007; resubmission received February 26, 2008; revised resubmission received March 25, 2008; accepted March 26, 2008.

From the Cardiovascular Division (M.M., A.Z., A.S., U.M., X.Y., Y.H., Q.X.), King's College, London; Department of Cardiac and Vascular Sciences (A.I.D.S.) and Department of Basic Medical Sciences (Y.-L.C.), St. George's, University of London, United Kingdom; Cancer Research UK Cambridge Research Institute (J.R.G., B.M.), United Kingdom; and Gaubius Laboratory and Leiden University Medical Center (P.H.Q.), The Netherlands.

Correspondence to Dr Manuel Mayr, Cardiovascular Division, The James Black Centre, King's College, University of London, 125 Coldharbour Ln, London SE5 9NU, United Kingdom. E-mail manuel.mayr@kcl.ac.uk

Circulation Research **is available at http://circres.ahajournals.org** **DOI: 10.1161/CIRCRESAHA.108.174623**

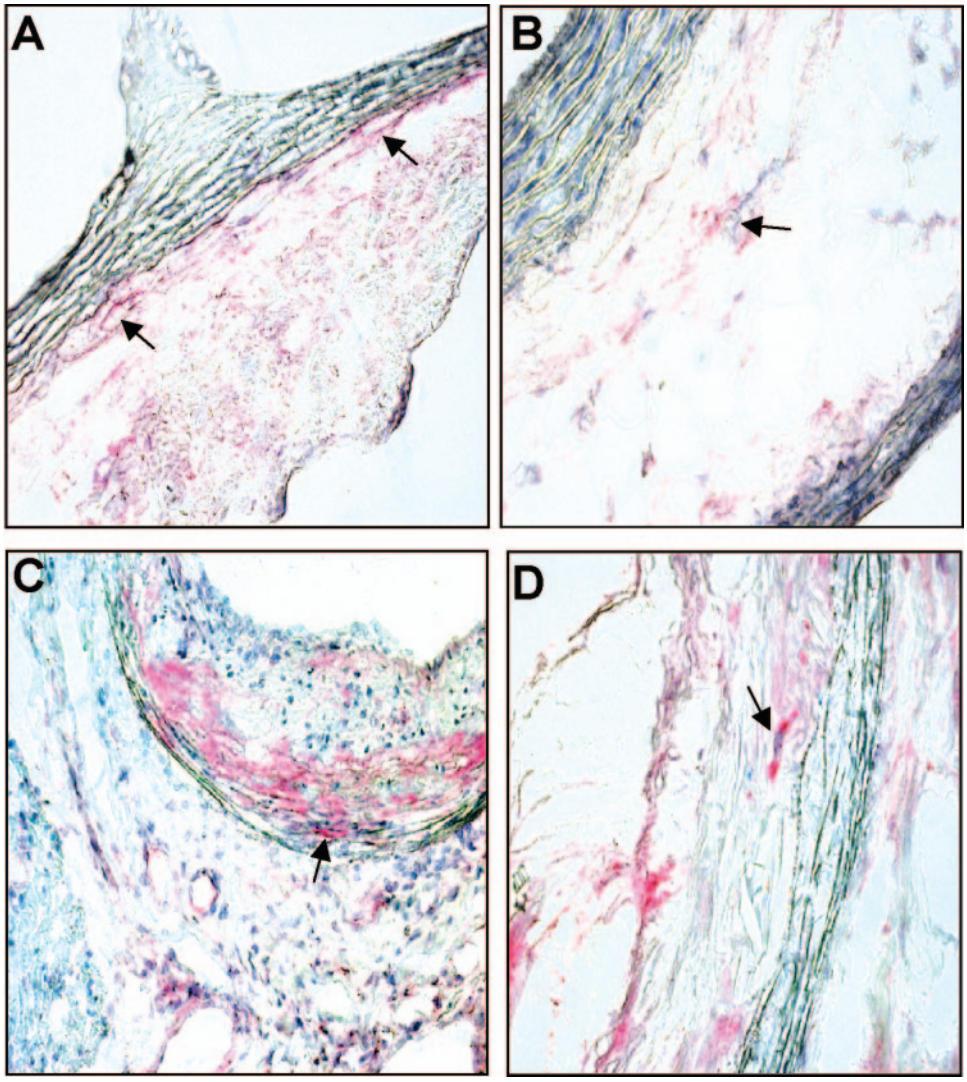

Figure 1. Sca-1$^+$ progenitors participate in atherosclerosis. Aortic roots from 10-week-old (A and B) and 12-month-old (C and D) apoE$^{-/-}$ mice were sectioned and labeled with anti–Sca-1 antibodies. Sections were developed with alkaline phosphatase anti–alkaline phosphatase (APAAP) techniques and counterstained with hematoxylin (blue). Arrows highlight Sca-1$^+$ cells. Note that Sca-1$^+$ cells are predominantly detectable in early (C) rather than complex (D) atherosclerotic lesions.

ics to demonstrate that Sca-1$^+$ progenitors derived from embryonic stem cells can express a panel of SMC markers in response to PDGF-BB stimulation without acquiring a mature SMC phenotype.[18] Instead, these SMC-like cells maintained characteristics of their embryonic stem cell origin.[19] Consequently, the question arose as to whether SMCs derived from adult progenitor cells in the adventitia of apoE$^{-/-}$ mice would be more similar to mature aortic SMCs. Because the phenotype of progenitor–derived cells is better reflected in their instantaneous protein profiles than the expression of a selected panel of marker proteins,[20] we compared the proteome of SMCs derived from adult Sca-1$^+$ progenitors with aortic SMCs derived from apoE$^{-/-}$ and apoE$^{+/+}$ mice by using difference in-gel electrophoresis (DIGE) and tandem mass spectrometry.

Materials and Methods

An expanded Materials and Methods section is available in the online data supplement http://circres.ahajournals.org.

Key techniques involved adaptations of previously published protocols, including those for the culture of SMCs,[21] the isolation of Sca-1$^+$ progenitors from the aortic adventitia,[13] differentiation of embryonic stem cells into SMC-like cells,[18] immunohistochemistry,[7] 2D gel electrophoresis,[22] tandem mass spectrometry,[23] NMR spectroscopy,[23] and RNase Protection assay.[24] Protocols for proteomic analysis are available on our web site at http://www.vascular-proteomics.com.

Results

Resident Sca-1$^+$ cells contribute to atherogenesis in apoE$^{-/-}$ mice. Sca-1$^+$ cells resided within the adventitia of aortas from 10-week-old apoE$^{-/-}$ mice (Figure 1A and 1B) but not apoE$^{+/+}$ mice.[13] Their recruitment to the vasculature coincided with increased expression of the CXC chemokine stromal cell–derived factor (SDF)-1α[25]: real-time PCR measurements revealed that the SDF-1α/GAPDH ratio was 0.97±0.12 and 0.74±0.10 in aortas of apoE$^{-/-}$ and apoE$^{+/+}$ mice, respectively (n=4, P=0.028). On cholesterol feeding, Sca-1$^+$ cells also appeared in the

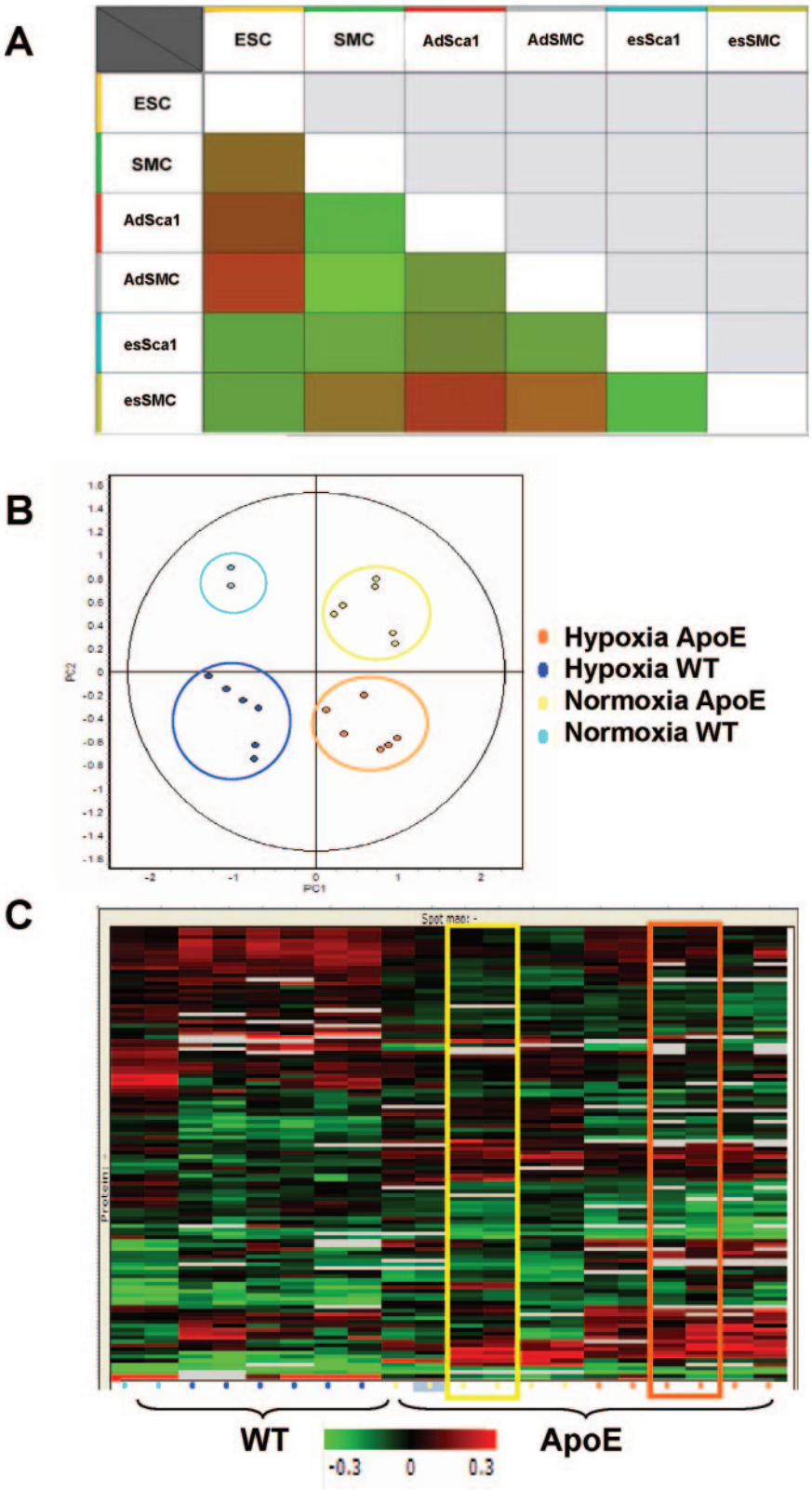

Figure 2. Proteomic characterization of SMCs and their vascular progenitors. A, Match matrix highlighting similarity between proteomic profiles of Sca-1$^+$ progenitors derived from embryonic stem cells or isolated from the adventitia of adult mice before and after PDGF-BB treatment. Bright green color denotes similarity; brown and red color, dissimilarity. Note that under PDGF-BB treatment, Sca1$^+$ progenitors from adult mice, but not from embryonic stem cells, resemble a mature SMC phenotype. ESC indicates embryonic stem cells; SMC, mature aortic SMCs; AdSca1, Sca-1$^+$ progenitors derived from the adventitia; AdSMC, adventitial Sca-1$^+$ progenitors after PDGF-BB stimulation; esSca1$^+$, Sca-1$^+$ progenitors derived from murine embryonic stem cells; esSMCs, embryonic stem cell–derived Sca-1$^+$ progenitors after PDGF-BB stimulation. The score plot in B shows a principal component analysis of proteomic profiles from SMCs derived from adult Sca-1$^+$ progenitors and from aortic SMCs of apoE$^{+/+}$ (Wt) and apoE$^{-/-}$ (apoE) mice under normoxic and hypoxic conditions. The black ellipse represents the 95% significance level. C, Hierarchical clustering was applied to rearrange the dataset. The spot maps in each experimental group were divided into 4 clusters. All apoE$^{+/+}$ and apoE$^{-/-}$ SMCs were closely grouped. Furthermore, there was a clear separation between hypoxia and normoxia. Moreover, SMCs derived from adventitial Sca1$^+$ progenitors (boxed lanes) were grouped with apoE$^{-/-}$ SMCs. X-axis indicates spot maps; y-axis, proteins. Red color denotes increase; green color, decrease. Black color indicates no change. Bar shows the log standard abundance value interval for the colors; ±0.3 denotes proteins with 3-fold increase or decrease.

adventitia of apoE$^{+/+}$ mice but fewer compared with apoE$^{-/-}$ mice (data not shown). During atherogenesis, numerous Sca-1$^+$ progenitors were present in early lesions (Figure 1C), whereas they were scarce in complex atheroma of 12-month-old apoE$^{-/-}$ mice (Figure 1D). Nonetheless, even in advanced lesions, there were almost twice as many cells staining for Sca-1 (≈2.3±0.9% of total lesional cells of the aortic root) compared with other progenitor cell markers, including c-kit (1.1±0.3%), CD34 (1.6±0.5%), and fetal liver kinase 1 (0.4±0.3%). No staining was observed for the embryonic stem cell marker SSEA-1 (data not shown).

Proteomic Characterization of Progenitor Cell–Derived SMCs

To get a better understanding of their biological potential, Sca-1$^+$ resident progenitor cells were isolated from the adventitia as described previously[13] and characterized by proteomics. For comparison, Sca-1$^+$ progenitors were also prepared from embryonic stem cells.[18,26] As indicated by the match matrix of their proteomic profiles (Figure 2A), the similarity of Sca-1$^+$ progenitors to mature aortic SMCs was independent of their vascular or embryonic origin. Unlike Sca-1$^+$ progenitors derived from embryonic stem cells, however, the proteome of adventitial Sca-1$^+$ cells closely resembled mature SMCs after PDGF-BB treatment. To accurately quantify differences in protein expression, we compared apoE$^{+/+}$, apoE$^{-/-}$, and Sca-1$^+$–derived SMCs under normoxia and hypoxia (18 hours, 5% O_2 balanced with N_2) using DIGE. Principal component analysis (Figure 2B) and hierarchical clustering (Figure 2C) revealed that after in vitro differentiation with PDGF-BB, the proteome of adult Sca-1$^+$ progenitors was reminiscent of their apoE$^{-/-}$ origin.

Proteomic Comparison of ApoE$^{-/-}$ SMCs Under Normoxia

Among the differentially expressed proteins (n=6, supplemental Figure I and supplemental Table I) were chaperones and endoplasmic reticulum proteins of the unfolded protein response quality-control system (UPR), such as erp29/Bip, glucose-regulated protein 78 and 94 (grp78, grp94), and protein disulfide isomerases A3 and A6. The UPR system has previously been shown to be activated at all stages of atherosclerosis in apoE$^{-/-}$ mice.[27] It reduces new protein synthesis by translational attenuation and eliminates misfolded proteins by the ubiquitin proteasome system. This is consistent with the observed downregulation of enzymes involved in amino acid metabolism and eukaryotic elongation factors, eEF1 delta and eEF2. The latter mediates the translocation step of elongation and is phosphorylated by a calcium- and calmodulin-dependent protein kinase regulated by insulin through the rapamycin-sensitive mTOR pathway.[28] When the differentially expressed proteins (n=51) were submitted to Ingenuity Pathway Analysis (Ingenuity System, Mountain View, Calif), the computational algorithms built 3 protein association networks (supplemental Figure II) and returned downregulation of amino acid metabolism and upregulation of glycolysis/glucose metabolism as the top canonical pathways.

Proteomic Comparison of ApoE$^{-/-}$ SMCs Under Hypoxia

Protein changes in hypoxic (n=12) compared with normoxic (n=8) SMCs are summarized in supplemental Figure III and supplemental Table II. In all cell lines, hypoxia induced an upregulation of glycolytic enzymes, as well as lactate dehydrogenase, with a concomitant downregulation of the pyruvate dehydrogenase complex, the bridge between aerobic and anaerobic glucose metabolism (supplemental Figure IV). Key enzymes of alternative glucose pathways, however, were predominantly upregulated in mature and progenitor-derived apoE$^{-/-}$ SMCs, ie, aldose reductase for the sorbitol pathway

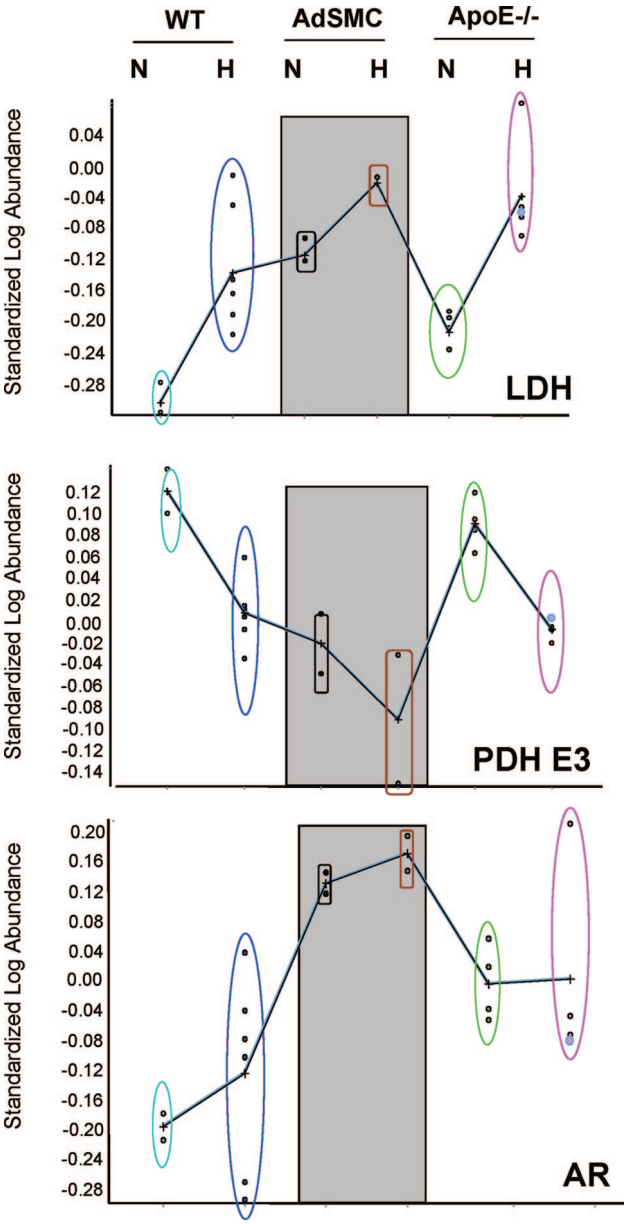

Figure 3. Representative enzymatic changes. Key enzymes in glucose metabolism were differentially expressed in wild-type (Wt), apoE$^{-/-}$, and adventitial progenitor-derived SMCs (AdSMC) under normoxic (N) and hypoxic (H) conditions. Note that the pattern for lactate dehydrogenase (LDH), dihydrolipoyl dehydrogenase (PDH E3), and aldose reductase (AR) in AdSMCs is more similar to mature apoE$^{-/-}$ SMCs than wild-type controls.

(Figure 3). The metabolic alterations in apoE-deficient SMCs were associated with an increase of transaldolase, the reversible link between glycolysis and the pentose phosphate pathway, as well as isoforms of cytosolic malate dehydrogenase and aspartate aminotransferase, the 2 enzymatic components of the malate-aspartate shuttle, which is responsible for transporting reducing equivalents from glycolysis into mitochondria. In addition, several of the differentially expressed proteins identified in normoxic apoE$^{-/-}$ SMCs were confirmed after hypoxia and their quantitative differences were almost identical in the 2 independent proteomic datasets, eg, for ezrin, fascin, annexin A2, and eEF2 (supplemental Figure

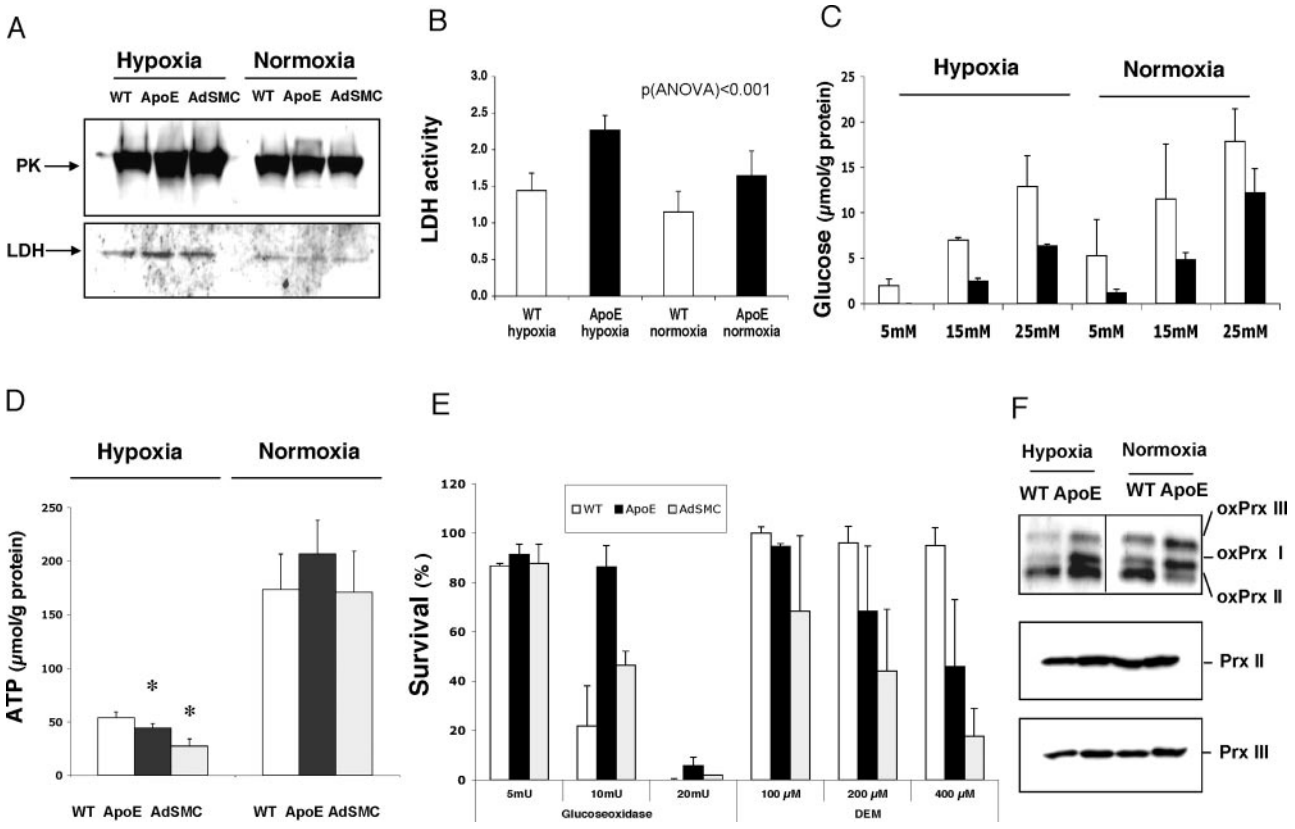

Figure 4. Glucose metabolism. A, Protein extracts of wild-type (Wt) and apoE$^{-/-}$ SMCs were probed with antibodies to pyruvate kinase (PK) and lactate dehydrogenase (LDH). B through D, Lactate dehydrogenase activity (B), glucose depletion in the culture medium (C), and cellular ATP (D), as measured under normoxic and hypoxic conditions. E, Increased susceptibility to oxidative stress–induced cell death. Survival of wild-type (white bars), apoE$^{-/-}$ SMCs (black bars), and progenitor-derived SMCs (gray bar) after incubation with glucose oxidase or diethylmaleate (DEM) in high glucose medium (25 mmol/L) for 24 hours is shown. Significant difference from controls: *$P<0.05$, **$P<0.01$. F, Oxidation of redox-sensitive proteins. Peroxiredoxins are a family of antioxidants that act by being the reducing substrate itself. Differences in the sulfoxidation of cytosolic (I, II) and mitochondrial (III) peroxiredoxins, as quantified by specific antibodies recognizing only the oxidized isoforms. No difference was observed for total Prx II and III.

V and supplemental Table III). Thus, cellular differences persisted in hypoxia, but enzymatic changes became more pronounced.

Immunoblotting and Enzymatic Assays

Consistent with our proteomic experiment, pyruvate kinase and lactate dehydrogenase increased in both apoE$^{+/+}$ and apoE$^{-/-}$ SMCs after hypoxia (Figure 4A), with the latter showing a tendency toward even higher levels. Despite similar net enzyme concentrations under normoxia, lactate dehydrogenase activity (Figure 4B) and glucose consumption (Figure 4C) were elevated in apoE$^{-/-}$ SMCs. ATP levels were similar to apoE$^{+/+}$ SMCs under normoxic conditions but lower in apoE$^{-/-}$ SMCs and progenitor-derived SMCs after hypoxia (Figure 4D). Compared with wild-type controls, apoE$^{-/-}$ SMCs and their progenitors were resistant to treatment with glucose oxidase as substrate depletion in the culture medium protected them against glucose oxidase–mediated oxidative injury (Figure 4E). They were, however, more susceptible to cell death in response to other oxidative stress stimuli,[7] ie, lowering the intracellular antioxidant glutathione by treatment with diethylmaleate (Figure 4E), and increased free radical generation in apoE$^{-/-}$ SMCs was evidenced by oxidation of redox-sensitive proteins, such as peroxiredoxins, providing additional confirmation of our proteomic data (supplemental Table III and Figure 4F).

Metabolomic Comparison of apoE$^{-/-}$ SMCs

To further clarify the metabolic effects of apoE deficiency, we measured metabolites in cellular extracts of normoxic SMCs cultivated in normal (5 mmol/L) and high glucose concentrations (25 mmol/L) by high-resolution NMR spectroscopy.[23] Quantitative data are included as supplemental Table IV. High glucose concentrations (25 mmol/L) resulted in a rise of myoinositol, which is exchanged for sorbitol to maintain osmoregulation. Notably, lactate levels were higher in apoE$^{-/-}$ than apoE$^{+/+}$ SMCs, and carnitine, required for the import of long-chain fatty acids into mitochondria and for transporting acetyl-coenzyme A out of the mitochondria to avoid a fatty acid–induced block of glycolysis, decreased by normalizing glucose concentrations in the culture medium in apoE$^{-/-}$, but not apoE$^{+/+}$ SMCs.

The effect of hypoxia on SMC metabolites is summarized in supplemental Table V. Apart from glycolic acid, cellular metabolites were similar in hypoxic apoE$^{+/+}$ and apoE$^{-/-}$ SMCs. NMR spectroscopy, however, confirmed that apoE$^{-/-}$ SMCs consumed glucose faster than their wild-type controls, as indicated by a depletion of glucose in the conditioned

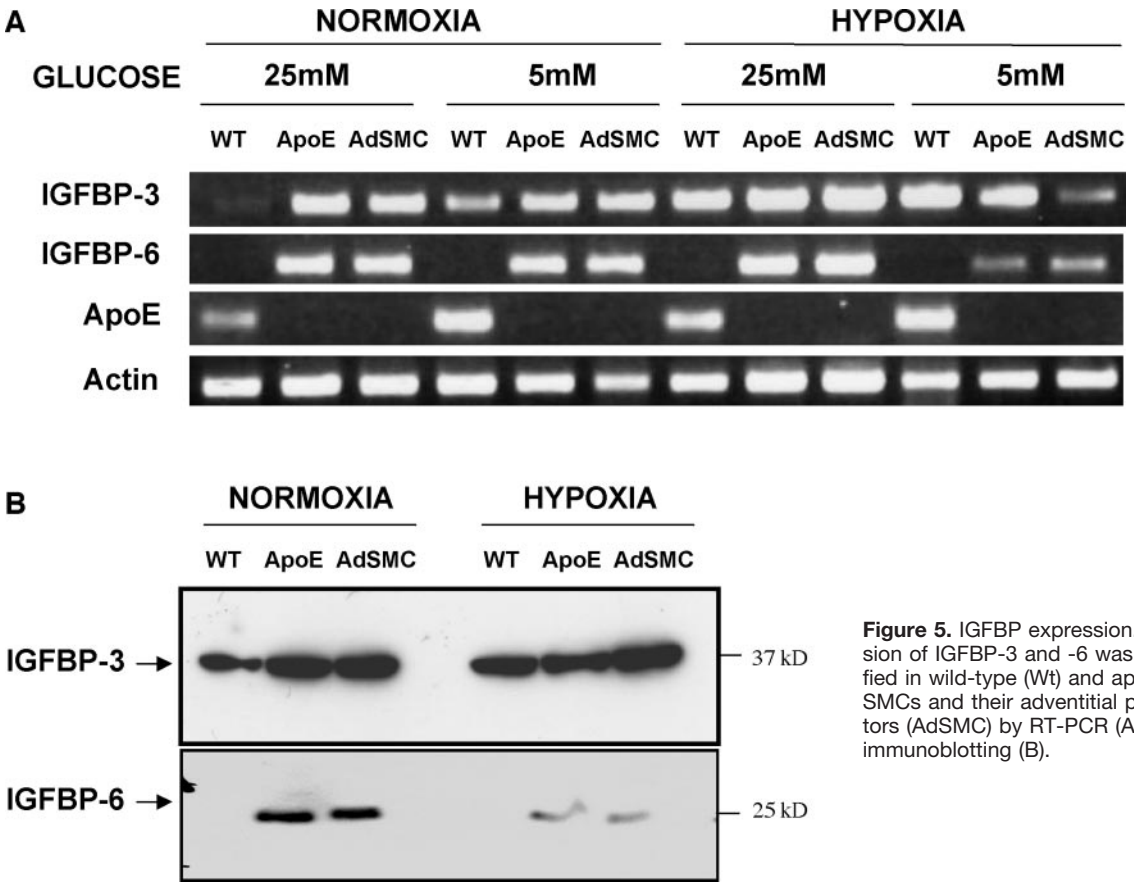

Figure 5. IGFBP expression. Expression of IGFBP-3 and -6 was quantified in wild-type (Wt) and apoE$^{-/-}$ SMCs and their adventitial progenitors (AdSMC) by RT-PCR (A) and immunoblotting (B).

medium and a corresponding rise in acetate, an endproduct of lipid metabolites (supplemental Figure VI). Thus, metabolism in apoE$^{-/-}$ SMCs was similar to hypoxic but not normoxic SMCs.

Interleukin-6 and Insulin-Like Growth Factor Binding Proteins

Apart from systemic factors, such as insulin, glucose metabolism is also regulated locally, ie, by the production of insulin-like growth factor (IGF) binding proteins (IGFBPs). We, therefore, evaluated IGFBP-1 to -7 expression in apoE$^{+/+}$, apoE$^{-/-}$, and progenitor-derived SMCs using RT-PCR. Whereas IGFBP-1 and -5 were undetectable in murine SMCs, expression of IGFBP-4 and -7 was identical in all cell lines. ApoE deficiency, however, was associated with a marked increase in IGFBP-3 and -6 at the mRNA (Figure 5A) and at the protein level (Figure 5B). Notably, IGFBP-3 was induced in apoE$^{+/+}$ SMCs by lowering glucose or oxygen concentrations in the culture medium, whereas IGFBP-6 was not inducible in wild-type SMCs despite its abundance in apoE$^{-/-}$ and progenitor-derived SMCs.

It has been demonstrated previously that tumor necrosis factor (TNF)-α regulates IGFBP-3 expression in SMCs.[29] Because TNF-α secretion was below detectable levels in the culture supernatant of murine SMCs (data not shown), we used a global approach (ie, RNase protection assay) to compare the capacity of wild-type, apoE$^{-/-}$, and progenitor-derived SMCs to produce other inflammatory mediators, including interleukin (IL)-1α, IL-1β, IL-1Ra, IL-6, IL-10, IL-12p35, IL12p40, IL-18, interferon-γ, and macrophage migration inhibitory factor. Expression was compared at baseline and after stimulation with bacterial lipopolysaccharides or TNF-α because apoE has been shown to suppress type I inflammatory responses in vivo.[30] Representative gels are shown in Figure 6. Whereas a transcriptional upregulation of interferon-inducible protein-10 and T-cell activation gene 3 was observed in apoE$^{-/-}$ SMCs and progenitor-derived SMCs after treatment with TNF-α and lipopolysaccharides, baseline mRNA transcripts for IL-18 were higher and for IL-6 lower in apoE$^{-/-}$ SMCs compared with wild-type controls. Subsequent measurements at the protein level confirmed a marked reduction of IL-6 secretion (Figure 7A, mean$\pm$SEM: 1.0$\pm$0.2 ng/mL in apoE$^{-/-}$ SMCs and 4.8$\pm$1.7 ng/mL in progenitor-derived SMCs versus 24.3$\pm$1.8 ng/mL in apoE$^{+/+}$ SMCs, respectively, $P<0.001$ [ANOVA]). Whereas glucose concentrations in the culture medium did not alter the baseline levels of IL-6 secretion in normoxic apoE$^{-/-}$ SMCs, the hypoxia-induced increase of IL-6 in apoE$^{-/-}$ SMCs was more pronounced in normal (5 mmol/L) than high (25 mmol/L) glucose medium (4.8 ng/mL versus 2.7 ng/mL, paired t test $P<0.05$). In contrast, glucose concentrations had no significant effect on the IL-6 release from hypoxic wild-type SMCs (data not shown). Thus, IL-6 secretion is substantially lower in apoE$^{-/-}$ SMCs but more responsive to glucose concentrations under hypoxia.

Next, we evaluated whether IL-6 would alter the IGFBP system. SMCs were incubated in fresh culture medium supplemented with 1 ng/mL and 10 ng/mL IL-6 for 24 hours.

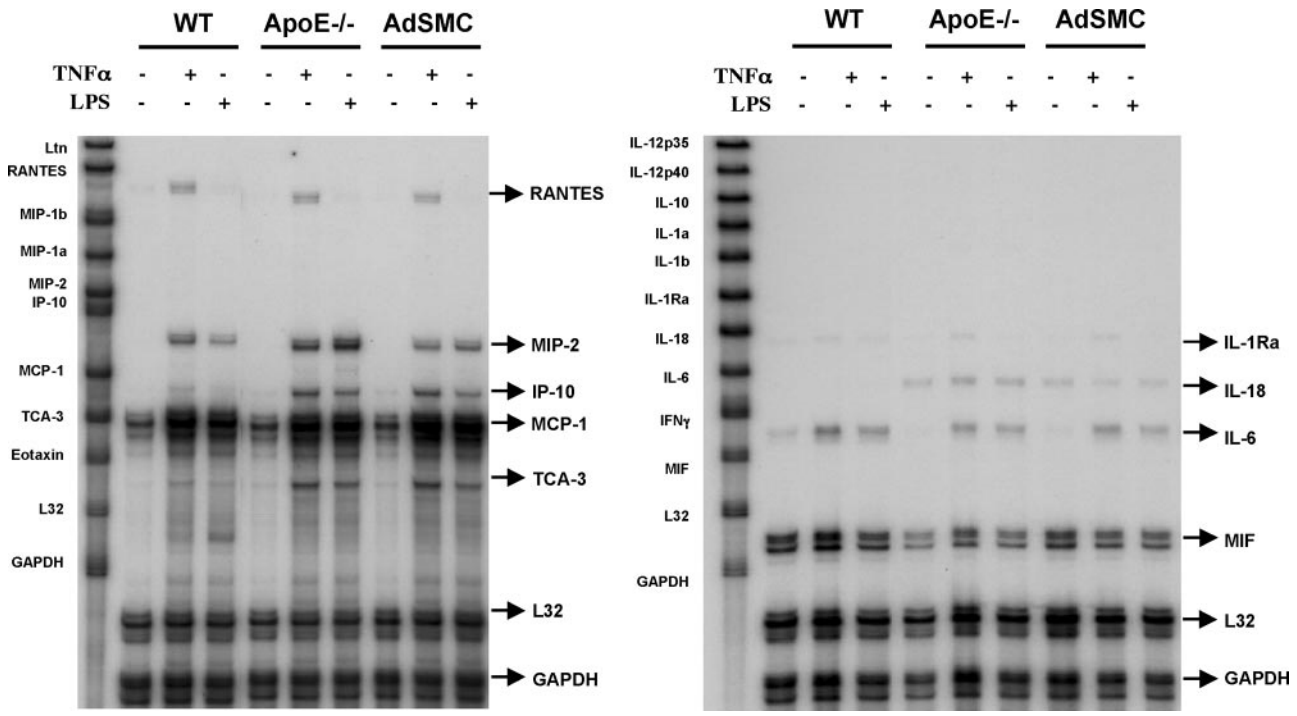

Figure 6. Cytokine expression. Total RNA was isolated from cells and analyzed by RNase Protection assay. GAPDH was used as a loading control.

Subsequently, mRNA transcripts for IGFBPs were quantified by RT-PCR. The administration of IL-6 resulted in transcriptional downregulation of IGFBP-3 and -6 but not other IGFBPs in apoE$^{-/-}$ and progenitor-derived SMCs (Figure 7B), demonstrating that the reduced levels of IL-6 account for the elevated IGFBP expression in apoE$^{-/-}$ SMCs.

IGFBPs in ApoE$^{+/+}$ SMCs From Hypercholesterolemic Mice

To establish whether the observed alterations resulted from apoE deficiency or hypercholesterolemia, we isolated aortic SMCs from cholesterol-fed wild-type mice. In these cells, too, a downregulation of apoE and IL-6 was associated with an upregulation of IGFBP-3 and IGFBP-6, confirming our concept of coregulation of apoE, IL-6 and IGFBPs (Figure 8A and 8B). Next, we silenced apoE expression using small interfering (si)RNA technology: downregulation of apoE by RNA interference was sufficient to reduce IL-6 secretion and to elevate IGFBP-6 expression in SMCs from normocholesterolemic mice. IGFBP-3, however, was not affected (Figure 8A and 8C). Thus, the observed phenotype in apoE$^{-/-}$ SMCs is probably the result of a combined effect of apoE deficiency and hypercholesterolemia.

Discussion

Possible roles of local progenitor cell populations within the vessel wall include a physical reconstruction of tissue during vascular repair, a paracrine support for growth of endogenous cells, or a limitation of inflammation. In the present study, we demonstrate that resident Sca-1^{+} cells migrate from the adventitia to the media during early atherosclerosis until they finally blend into the tissue in more complex lesions. Using a proteomic approach, we established that these adult progenitors have the potential of acquiring a mature SMC phenotype: unlike Sca-1^{+} progenitors derived from embryonic stem cells, Sca-1^{+} cells from the adventitia of aortas of apoE$^{-/-}$ mice had protein profiles similar to aortic SMCs after incubation with PDGF-BB in vitro. Notably, they maintained functional alterations indicative of their apoE$^{-/-}$ origin, as evidenced by their accelerated glucose consumption, increased transcription of IL-18, decreased synthesis of IL-6, elevated expression of IGFBP-3 and -6, and their susceptibility to oxidative stress. Thus, our data support the possibility of a physical incorporation of adult progenitors in the vasculature, although their overall similarity to mature apoE$^{-/-}$ SMCs, especially with respect to cytokine profiles, argues against a paracrine support or a limiting effect on inflammation.

Metabolism in ApoE$^{-/-}$ SMCs

In our previous proteomic and metabolomic analysis of aortas from apoE$^{-/-}$ mice,[31] we demonstrated that inefficient energy metabolism and increased oxidative stress preceded atherosclerotic lesion formation in hyperlipidemic animals. It is well established that oxygen consumption in the vasculature is augmented by accumulation of inflammatory cells and that lipid deposition in the arteries reduces the diffusion distance of oxygen and water soluble metabolites such as glucose, the main source of energy for the vasculature. Interestingly, cultivated aortic SMCs from apoE$^{-/-}$ mice showed accelerated glucose consumption and increased susceptibility to oxidative stress. Notably, the hyperglycemia-induced downregulation of the glucose transport is important for protecting cells against an excessive influx of glucose, a key factor for oxidative stress.

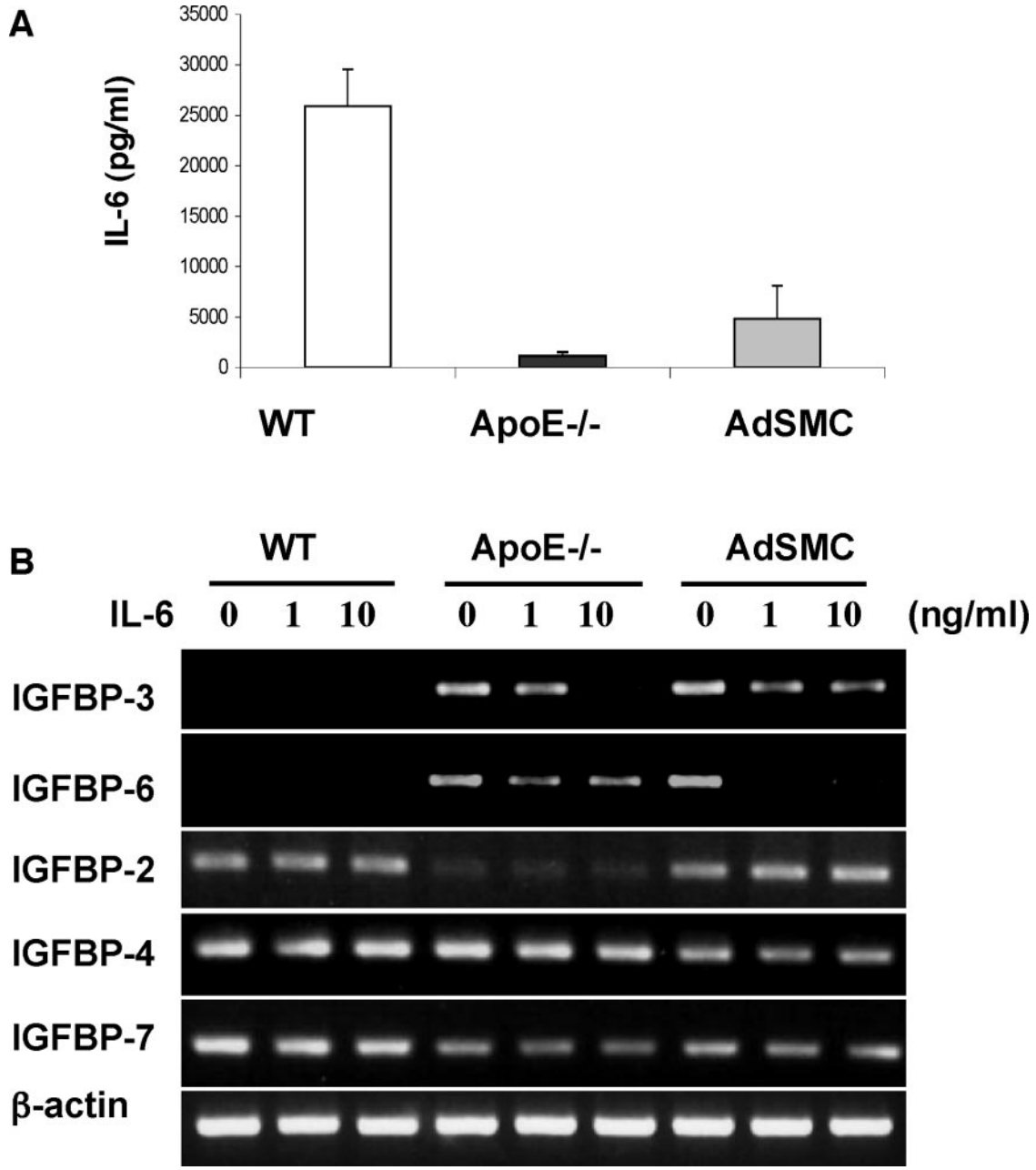

Figure 7. IL-6 attenuates IGFBP expression. A, IL-6 concentration in the conditioned medium. B, Effect of IL-6 supplementation on IGFBP expression.

Insulin-Like Growth Factor Binding Proteins

Glucose metabolism is modulated by insulin sensitivity in the target tissue. IGF-1 is a potent hypoglycemic agent with a similar function to insulin and an important survival factor for SMCs in atherosclerotic lesions.[32,33] Unlike insulin, the bioavailability of IGF in the circulation and in the extracellular space is regulated by IGFBPs, which are produced by local tissues and modulate IGF-1 effects.[32] Whereas liver-derived IGFBP-1 is the main binding partner for IGF-1 in the circulation and IGFBP-1 circulating levels correlate negatively with cardiovascular disease, IGFBP-3 has a similar ability to bind IGF-1 but is also produced in local tissues and plasma levels increase in patients with cardiovascular disease.[34] Notably, IGFBP-3 has intrinsic bioactivity and has recently been implicated in the differentiation of hematopoietic progenitors during vascular development.[35] In this respect, it is noteworthy that IL-6 supplementation normalized IGFBP-3 levels faster than IGFBP-6 in progenitor-derived SMCs, whereas the opposite was the case in mature apoE$^{-/-}$ SMCs (Figure 7B).

The expression, secretion, and regulation of IGFBPs in SMCs are known to be species specific: rat and murine wild-type SMCs expressed predominantly mRNA transcripts for IGFBP-2 and 4.[36] Whereas angiotensin II, thrombin, and reactive oxygen species reduced levels of IGFBP-4, IGFBP-2 and IGFBP-4 significantly increased in response native LDL and oxidized LDL and TNF-α induced IGFBP-3.[29,32,36] The present study is, to our knowledge, the first evidence that

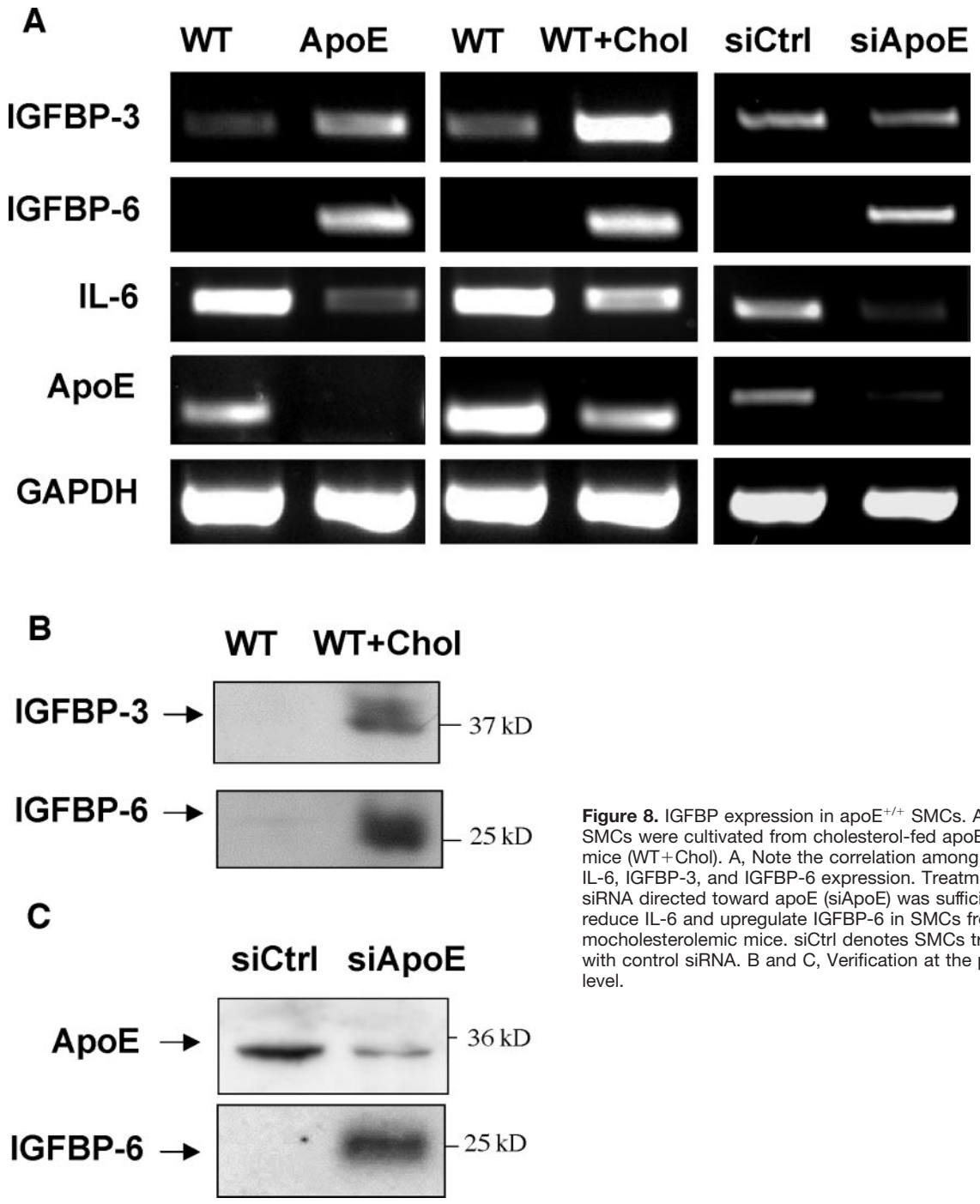

Figure 8. IGFBP expression in apoE$^{+/+}$ SMCs. Aortic SMCs were cultivated from cholesterol-fed apoE$^{+/+}$ mice (WT+Chol). A, Note the correlation among apoE, IL-6, IGFBP-3, and IGFBP-6 expression. Treatment with siRNA directed toward apoE (siApoE) was sufficient to reduce IL-6 and upregulate IGFBP-6 in SMCs from normocholesterolemic mice. siCtrl denotes SMCs treated with control siRNA. B and C, Verification at the protein level.

glucose depletion and hypoxia stimulate the expression of IGFBP-3, whereas the same stimuli had no effect on IGFBP-6. Both, IGFBP-3 and IGFBP-6, however, were upregulated in apoE$^{-/-}$ SMCs and progenitor-derived SMCs. This phenotype was replicated in apoE$^{+/+}$ SMCs from cholesterol-fed mice. To exclude that our findings were attributable to an inflammatory response following chronic hypercholesterolemia, we silenced apoE expression in wild-type SMCs from normocholesterolemic mice: in this experiment, too, downregulation of apoE was accompanied by decreased IL-6 production and a rise in IGFBP-6. Only IGFBP-3 was unchanged. These findings are consistent with our observations that IGFBP-3 is more responsive to environmental factors, ie, glucose and oxygen concentrations in the culture medium, and less dependent on the expression levels of apoE than IGFBP-6 (Figure 5). As summarized in supplemental Table VI, we demonstrated by 3 different methods (ie, by feeding a cholesterol-rich diet, by RNA interference, and by deleting the endogenous gene) that a reduction of apoE expression in SMCs resulted in a downregulation of IL-6 and a corresponding rise in IGFBP expression, which was reversible by supplementing IL-6 to the culture medium. Thus, we provide clear evidence that chronic hypercholesterolemia has lasting metabolic effects on SMCs, which are not only

attributable to the inflammatory response in the vasculature but also influenced by the expression levels of apoE.

Metabolic Effects of Cytokines

Although metabolic disturbances are recognized as a key factor in both the initiation and progression of atherosclerosis, inflammatory cytokines are predominantly studied in the context of inflammation and their pronounced metabolic actions that contribute to the general adaptation of the organism during inflammatory stress are attracting less attention in cardiovascular research. IL-6 is known to play a key role in the immune and acute phase response. IL-6 expression is higher in atherosclerotic than normal arteries, and injection of IL-6 accelerates atherosclerosis in apoE$^{-/-}$ mice.[37] In addition to its potent inflammatory properties, however, IL-6 may have profound metabolic effects in vascular SMCs. In skeletal muscle, for example, IL-6 has been implicated as "exercise factor"[38,39] that acts in a paracrine manner on neighboring muscle cells and is released within minutes. The depletion of glycogen stores within muscle fibers triggers the release of IL-6 to increase glucose supply by stimulating lipolysis in the adipose tissue and glycogen breakdown in the liver.[39] In contrast to TNF-α, IL-6 does not make cells insensitive to insulin but stimulates glucose uptake and the rise of IL-6 during prolonged exercise can become as high as in sepsis.

Atherosclerotic lesions occur at preferential sites along the vasculature, and increased metabolic demand may explain why specific hemodynamic conditions initiate disease at these particular locations but not in their vicinity. We have demonstrated recently that mechanical stretch is a potent inducer of IL-6 in vascular SMCs.[24] We now report that IL-6 secretion is inversely correlated with glucose consumption: wild-type SMCs consumed less glucose but secreted more IL-6, whereas high glucose turnover in apoE$^{-/-}$ SMCs and progenitor-derived SMCs was associated with low levels of IL-6 secretion. Moreover, their hypoxia-induced increase in IL-6 secretion was attenuated by higher glucose concentrations in the culture medium, indicating that substrate availability constitutes an important factor determining cytokine release. By regulating IGFBP synthesis and modulating IGF availability, IL-6 may constitute an integral component of the inflammatory–metabolic interplay in vascular SMCs.

IL-18 is another important regulator in the homeostasis of energy intake.[40] IL-18$^{-/-}$ mice showed insulin resistance at the level of muscle and adipose tissue and increased fat deposition in the arterial walls.[40] Like IL-6,[37] IL-18 administration accelerated atherosclerosis in apoE$^{-/-}$ mice.[41] Moreover, a double knockout for IL-18 and apoE had reduced atherosclerosis despite higher cholesterol levels,[42] and overexpression of an IL-18 binding protein in apoE$^{-/-}$ mice prevented lesion development and promoted a stable plaque phenotype.[43] The increase in IL-18 transcription, as observed in the present study, is consistent with a recent report that apoE is a negative regulator of IL-18.[44] Overall, it is apparent that cytokines not only regulate immune or inflammatory responses in atherosclerosis but also contribute to glucose homeostasis[45] in the SMC compartment.

Therapeutic Potential of Resident Progenitor Cells

Our findings demonstrate that resident Sca-1^{+} progenitors from the aortic adventitia are a viable source of vascular SMCs and differentiate more readily toward the vascular SMC lineage than embryonic stem cell–derived progenitors. Remarkably, they shared many characteristics of apoE$^{-/-}$ SMCs, including their increased susceptibility to oxidative stress, although Sca-1^{+} cells were harvested from disease-free aortas of young apoE$^{-/-}$ mice and differentiated to SMCs in a normolipidemic environment. These data suggest that the deletion of the apoE gene has effects that extend beyond SMC differentiation to the progenitor level. In addition, besides reducing the number of circulating progenitors, vascular risk factors, such as hypercholesterolemia, may also influence the differentiation and regenerative potential of local stem cell populations, ie, by increasing hypoxia-regulated factors such as IGFBP-3,[35] a recently identified modulator of vascular survival and regrowth in an oxygen-deprived environment.[46]

Summary

By integrating multiple phenotypic facets of mature and progenitor cell-derived SMCs from hyperlipidemic mice, we illustrate how changes in the proteome, the secretome, and the metabolome are reciprocally connected and how proteomics offers an opportunity to progress toward a molecular classification of stem cell–derived cells.

Sources of Funding

The use of the facilities of the Medical Biomics Centre at St. George's, University of London, is gratefully acknowledged. This work was supported by grants from the British Heart Foundation and the Oak Foundation.

Disclosures

None.

References

1. Meir KS, Leitersdorf E. Atherosclerosis in the apolipoprotein E-deficient mouse: a decade of progress. *Arterioscler Thromb Vasc Biol*. 2004;24:1006–1014.
2. Duan H, Li Z, Mazzone T. Tumor necrosis factor-alpha modulates monocyte/macrophage apoprotein E gene expression. *J Clin Invest*. 1995;96:915–922.
3. Moore ZW, Zhu B, Kuhel DG, Hui DY. Vascular apolipoprotein e expression and recruitment from circulation to modulate smooth muscle cell response to endothelial denudation. *Am J Pathol*. 2004;164:2109–2116.
4. Majack RA, Castle CK, Goodman LV, Weisgraber KH, Mahley RW, Shooter EM, Gebicke-Haerter PJ. Expression of apolipoprotein E by cultured vascular smooth muscle cells is controlled by growth state. *J Cell Biol*. 1988;107:1207–1213.
5. Ishigami M, Swertfeger DK, Granholm NA, Hui DY. Apolipoprotein E inhibits platelet-derived growth factor-induced vascular smooth muscle cell migration and proliferation by suppressing signal transduction and preventing cell entry to G1 phase. *J Biol Chem*. 1998;273:20156–20161.
6. Zhu B, Kuhel DG, Witte DP, Hui DY. Apolipoprotein E inhibits neointimal hyperplasia after arterial injury in mice. *Am J Pathol*. 2000;157:1839–1848.
7. Dietrich H, Hu Y, Zou Y, Huemer U, Metzler B, Li C, Mayr M, Xu Q. Rapid development of vein graft atheroma in ApoE-deficient mice. *Am J Pathol*. 2000;157:659–669.
8. Zhang SH, Reddick RL, Burkey B, Maeda N. Diet-induced atherosclerosis in mice heterozygous and homozygous for apolipoprotein E gene disruption. *J Clin Invest*. 1994;94:937–945.

9. Hillebrands JL, Klatter FA, van den Hurk BM, Popa ER, Nieuwenhuis P, Rozing J. Origin of neointimal endothelium and alpha-actin-positive smooth muscle cells in transplant arteriosclerosis. *J Clin Invest*. 2001; 107:1411–1422.
10. Saiura A, Sata M, Hirata Y, Nagai R, Makuuchi M. Circulating smooth muscle progenitor cells contribute to atherosclerosis. *Nat Med*. 2001;7: 382–383.
11. Simper D, Stalboerger PG, Panetta CJ, Wang S, Caplice NM. Smooth muscle progenitor cells in human blood. *Circulation*. 2002;106: 1199–1204.
12. Hu Y, Davison F, Ludewig B, Erdel M, Mayr M, Url M, Dietrich H, Xu Q. Smooth muscle cells in transplant atherosclerotic lesions are originated from recipients, but not bone marrow progenitor cells. *Circulation*. 2002; 106:1834–1839.
13. Hu Y, Zhang Z, Torsney E, Afzal AR, Davison F, Metzler B, Xu Q. Abundant progenitor cells in the adventitia contribute to atherosclerosis of vein grafts in ApoE-deficient mice. *J Clin Invest*. 2004;113: 1258–1265.
14. Hu Y, Mayr M, Metzler B, Erdel M, Davison F, Xu Q. Both donor and recipient origins of smooth muscle cells in vein graft atherosclerotic lesions. *Circ Res*. 2002;91:e13–e20.
15. Mayr M, Li C, Zou Y, Huemer U, Hu Y, Xu Q. Biomechanical stress-induced apoptosis in vein grafts involves p38 mitogen-activated protein kinases. *FASEB J*. 2000;14:261–270.
16. Mayr M, Hu Y, Hainaut H, Xu Q. Mechanical stress-induced DNA damage and rac-p38MAPK signal pathways mediate p53-dependent apoptosis in vascular smooth muscle cells. *FASEB J*. 2002;16:1423–1425.
17. Mayr U, Mayr M, Li C, Wernig F, Dietrich H, Hu Y, Xu Q. Loss of p53 accelerates neointimal lesions of vein bypass grafts in mice. *Circ Res*. 2002;90:197–204.
18. Yin X, Mayr M, Xiao Q, Wang W, Xu Q. Proteomic analysis reveals higher demand for antioxidant protection in embryonic stem cell-derived smooth muscle cells. *Proteomics*. 2006;6:6437–6446.
19. Sidibe A, Yin X, Tarelli E, Xiao Q, Zampetaki A, Xu Q, Mayr M. Integrated membrane protein analysis of mature and embryonic stem cell-derived smooth muscle cells using a novel combination of CyDye/ biotin labeling. *Mol Cell Proteomics*. 2007;6:1788–1797.
20. Mayr M, Madhu B, Xu Q. Proteomics and metabolomics combined in cardiovascular research. *Trends Cardiovasc Med*. 2007;17:43–48.
21. Hu Y, Zou Y, Dietrich H, Wick G, Xu Q. Inhibition of neointima hyperplasia of mouse vein grafts by locally applied suramin. *Circulation*. 1999;100:861–868.
22. Mayr U, Mayr M, Yin X, Begum S, Tarelli E, Wait R, Xu Q. Proteomic dataset of mouse aortic smooth muscle cells. *Proteomics*. 2005;5: 4546–4557.
23. Mayr M, Siow R, Chung YL, Mayr U, Griffiths JR, Xu Q. Proteomic and metabolomic analysis of vascular smooth muscle cells: role of PKCdelta. *Circ Res*. 2004;94:e87–e96.
24. Zampetaki A, Zhang Z, Hu Y, Xu Q. Biomechanical stress induces IL-6 expression in smooth muscle cells via Ras/Rac1–p38 MAPK-NF-kappaB signaling pathways. *Am J Physiol Heart Circ Physiol*. 2005;288: H2946–H2954.
25. Schober A, Knarren S, Lietz M, Lin EA, Weber C. Crucial role of stromal cell-derived factor-1alpha in neointima formation after vascular injury in apolipoprotein E-deficient mice. *Circulation*. 2003;108:2491–2497.
26. Xiao Q, Zeng L, Zhang Z, Hu Y, Xu Q. Stem cell-derived Sca-1+ progenitors differentiate into smooth muscle cells, which is mediated by collagen IV-integrin alpha1/beta1/alphav and PDGF receptor pathways. *Am J Physiol Cell Physiol*. 2007;292:C342–C352.
27. Zhou J, Lhotak S, Hilditch BA, Austin RC. Activation of the unfolded protein response occurs at all stages of atherosclerotic lesion development in apolipoprotein E-deficient mice. *Circulation*. 2005;111:1814–1821.
28. Browne GJ, Proud CG. A novel mTOR-regulated phosphorylation site in elongation factor 2 kinase modulates the activity of the kinase and its binding to calmodulin. *Mol Cell Biol*. 2004;24:2986–2997.
29. Anwar A, Zahid AA, Scheidegger KJ, Brink M, Delafontaine P. Tumor necrosis factor-alpha regulates insulin-like growth factor-1 and insulin-like growth factor binding protein-3 expression in vascular smooth muscle. *Circulation*. 2002;105:1220–1225.
30. Ali K, Middleton M, Pure E, Rader DJ. Apolipoprotein E suppresses the type I inflammatory response in vivo. *Circ Res*. 2005;97:922–927.
31. Mayr M, Chung YL, Mayr U, Yin X, Ly L, Troy H, Fredericks S, Hu Y, Griffiths JR, Xu Q. Proteomic and metabolomic analyses of atherosclerotic vessels from apolipoprotein E-deficient mice reveal alterations in inflammation, oxidative stress, and energy metabolism. *Arterioscler Thromb Vasc Biol*. 2005;25:2135–2142.
32. Bayes-Genis A, Conover CA, Schwartz RS. The insulin-like growth factor axis: a review of atherosclerosis and restenosis. *Circ Res*. 2000; 86:125–130.
33. Bennett MR, Evan GI, Schwartz SM. Apoptosis of human vascular smooth muscle cells derived from normal vessels and coronary atherosclerotic plaques. *J Clin Invest*. 1995;95:2266–2274.
34. Kawachi S, Takeda N, Sasaki A, Kokubo Y, Takami K, Sarui H, Hayashi M, Yamakita N, Yasuda K. Circulating insulin-like growth factor-1 and insulin-like growth factor binding protein-3 are associated with early carotid atherosclerosis. *Arterioscler Thromb Vasc Biol*. 2005;25: 617–621.
35. Chang KH, Chan-Ling T, McFarland EL, Afzal A, Pan H, Baxter LC, Shaw LC, Caballero S, Sengupta N, Li Calzi S, Sullivan SM, Grant MB. IGF binding protein-3 regulates hematopoietic stem cell and endothelial precursor cell function during vascular development. *Proc Natl Acad Sci U S A*. 2007;104:10595–10600.
36. Delafontaine P, Song YH, Li Y. Expression, regulation, and function of IGF-1, IGF-1R, and IGF-1 binding proteins in blood vessels. *Arterioscler Thromb Vasc Biol*. 2004;24:435–444.
37. Huber SA, Sakkinen P, Conze D, Hardin N, Tracy R. Interleukin-6 exacerbates early atherosclerosis in mice. *Arterioscler Thromb Vasc Biol*. 1999;19:2364–2367.
38. Pedersen BK, Steensberg A, Fischer C, Keller C, Keller P, Plomgaard P, Febbraio M, Saltin B. Searching for the exercise factor: is IL-6 a candidate? *J Muscle Res Cell Motil*. 2003;24:113–119.
39. Keller C, Steensberg A, Pilegaard H, Osada T, Saltin B, Pedersen BK, Neufer PD. Transcriptional activation of the IL-6 gene in human contracting skeletal muscle: influence of muscle glycogen content. *FASEB J*. 2001;15:2748–2750.
40. Netea MG, Joosten LA, Lewis E, Jensen DR, Voshol PJ, Kullberg BJ, Tack CJ, van Krieken H, Kim SH, Stalenhoef AF, van de Loo FA, Verschueren I, Pulawa L, Akira S, Eckel RH, Dinarello CA, van den Berg W, van der Meer JW. Deficiency of interleukin-18 in mice leads to hyperphagia, obesity and insulin resistance. *Nat Med*. 2006;12:650–656.
41. Whitman SC, Ravisankar P, Daugherty A. Interleukin-18 enhances atherosclerosis in apolipoprotein E(−/−) mice through release of interferon-gamma. *Circ Res*. 2002;90:e34–e38.
42. Elhage R, Jawien J, Rudling M, Ljunggren HG, Takeda K, Akira S, Bayard F, Hansson GK. Reduced atherosclerosis in interleukin-18 deficient apolipoprotein E-knockout mice. *Cardiovasc Res*. 2003;59: 234–240.
43. Mallat Z, Corbaz A, Scoazec A, Graber P, Alouani S, Esposito B, Humbert Y, Chvatchko Y, Tedgui A. Interleukin-18/interleukin-18 binding protein signaling modulates atherosclerotic lesion development and stability. *Circ Res*. 2001;89:e41–e45.
44. Kawamura A, Baitsch D, Telgmann R, Feuerborn R, Weissen-Plenz G, Hagedorn C, Saku K, Brand-Herrmann SM, von Eckardstein A, Assmann G, Nofer JR. Apolipoprotein E interrupts interleukin-1beta signaling in vascular smooth muscle cells. *Arterioscler Thromb Vasc Biol*. 2007;27: 1610–1617.
45. Henderson JT, Mullen BJ, Roder JC. Physiological effects of CNTF-induced wasting. *Cytokine*. 1996;8:784–793.
46. Lofqvist C, Chen J, Connor KM, Smith ACH, Aderman CM, Liu N, Pintar JE, Ludwig T, Hellstrom A, Smith LEH. IGFBP3 suppresses retinopathy through suppression of oxygen-induced vessel loss and promotion of vascular regrowth. *Proc Natl Acad Sci U S A*. 2007;104: 10589–10594.

PROTEOMIC AND METABOLOMIC ANALYSIS OF SMOOTH MUSCLE CELLS DERIVED FROM THE ARTERIAL MEDIA AND ADVENTITIAL PROGENITORS OF APOLIPOPROTEIN E-DEFICIENT MICE

Manuel Mayr[1], Anna Zampetaki[1], Anissa Sidibe[1], Ursula Mayr[1], Xiaoke Yin[1], Ayesha I. De Souza[2], Yuen-Li Chung[3], Basetti Madhu[4], Paul H. Quax[5], Yanhua Hu[1], John R. Griffiths[4], Qingbo Xu[1]

[1] Cardiovascular Division, King's College, London

[2] Department of Cardiac and Vascular Sciences, St George´s, University of London, UK,

[3] Department of Basic Medical Sciences, St George´s, University of London, UK,

[4] Cancer Research UK Cambridge Research Institute, Cambridge, UK,

[5] Gaubius Laboratory and Leiden University Medical Center Leiden, The Netherlands

ONLINE SUPPLEMENT

Correspondence to:

Dr. Manuel Mayr, Cardiovascular Division,
The James Black Centre, King's College, University of London
125 Coldharbour Lane, London SE5 9NU, UK
Phone: +44 (0) 20 7848 5238
Fax: +44 (0) 20 7848 5296
Email: manuel.mayr@kcl.ac.uk

MATERIAL AND METHODS

Mice. All procedures were performed according to protocols approved by the Institutional Committee for Use and Care of Laboratory Animals. ApoE-deficient mice on a C57BL/6 background were purchased from Jackson Laboratories (West Grove, Pa) and maintained in our laboratory. $ApoE^{+/+}$ and $apoE^{-/-}$ mice were on a normal chow diet containing 4.5% fat by weight (0.02% cholesterol), kept on a light/dark (12/12h) cycle at 22°C receiving food and water *ad libitum*. For $apoE^{-/-}$ mice genotyping, a Jackson's PCR protocol was used with primers: oIMR180 5'- GCC TAG CCG AGG GAG AGC CG-3', oIMR181 5'- TGT GAC TTG GGA GCT CTG CAG C -3' and oIMR182 5'- GCC GCC CCG ACT GCA TCT -3'. 2 months-old $apoE^{+/+}$ mice were also fed a high-cholesterol diet for 8 weeks (1.25% cholesterol, 17% coconut butter, from Test diet, USA). Plasma cholesterol levels were measured by the cholesterol oxidase method (Sigma). The aortic root and a portion of the heart were harvested from 10 week-old and 12 month-old mice and frozen in liquid nitrogen.

Immunohistochemistry. The procedure used in the present study was similar to that described previously[1]. Briefly, serial 5-µm thick frozen sections of aortic roots were overlaid with rat monoclonal antibodies against mouse SSEA-1 (stage-specific embryonic antigen-1; MAB4301, Chemicon Europe, Hampshire, UK), sca-1 (stem cell antigen) (R&D Systems, Cat No. AF1226), c-kit (Pharmingen, cat No. 553352), CD31 (Abcam Ltd, Cambridge, UK, Cat No. ab7388), CD34 (Abcam Ltd, Cambridge, UK, Cat No. ab6330), Flk-1 (BD Biosiences Pharmingen, Cat No. 550549), MAC-1 (CD11b/18) (PharMingen, San Diego, CA) and alpha-actin (Sigma, C6198 and A5691). Sections were visualized with alkaline phosphatase-anti-alkaline phosphatase (APAAP) complex

(Dakopatts) and developed using a substrate solution (Sigma). The sections were counterstained with haematoxylin. Semi-quantitive evaluation was performed at 400x magnification. Positive stained cells in the vessel wall were counted and expressed as the range of the cell number or the percentage of total nuclei.

Cell culture. Mature SMCs were cultivated from aortas of 3 month-old apoE$^{+/+}$ and apoE-/- mice on normal chow diet as described previously[1,2]. Cell identity was routinely assessed by immunohistochemistry using antibodies specific to alpha smooth muscle actin and smooth muscle myosin. SMC marker expression was similar in cultured apoE$^{+/+}$ and apoE$^{-/-}$ SMCs (data not shown). Sca-1^{+} vascular progenitor cells were isolated from the adventitia of 3 months-old apoE$^{-/-}$ mice by magnetic cell sorting as described previously[3]. Stimulation by PDGF-BB (10ng/ml) for 5 passages resulted in mRNA expression of smooth muscle alpha-actin, SM22, calponin and smooth muscle myosin heavy chain. Verification by FACS analysis showed that the majority of Sca-1^{+}-derived SMCs expressed SMC markers[3]. For hypoxia, SMCs were seeded at a concentration of 1 x 10^6 for a T75 flask on day 1. On day 2, medium was be changed, and SMCs were divided into 2 groups; one group was placed in 1% O_2, 5% CO_2 balanced with N_2 for 18 hours while the other group was continued in the 95% air and 5% CO_2 incubator.

Differentiation of ES cells to SMCs. Murine ES cells (ES-D3 cell line, CRL-1934, ATCC) were maintained as described previously[4] in DMEM (ATCC) containing 10% fetal bovine serum (FBS, ATCC), 10ng/ml recombinant human leukaemia inhibitory factor (LIF, Chemicon), 0.1mM 2-mercaptoethanol (Sigma), 2mM L-glutamine (Invitrogen), 100U/ml Penicillin (Invitrogen), and 100μg/ml streptomycin

(Invitrogen). Undifferentiated ES cells were incubated at 37°C in a humidified atmosphere with 5% CO_2 and passaged into flasks coated with 0.04% gelatine (Sigma) at a ratio of 1:6 to 1:10 every 2 days. During the differentiation process, ES cells were first pre-differentiated in collagen type IV (Trevigen)-coated flasks for 3-4 days in basic differentiation medium (DM): α-minimal essential medium (α MEM, Invitrogen), supplemented with 10% FCS (Invitrogen), 50μM 2-mercaptoethanol (Sigma), 2mM L-glutamine (Invitrogen), 100U/ml Penicillin (Invitrogen), and 100μg/ml streptomycin (Invitrogen). Sca-1$^+$ cells were isolated by magnetic labelling cell sorting system (MACS) using anti-Sca-1 magnetic beads (Miltenyi Biotec) as described in our previous studies[3]. Sca-1$^+$ cells were resuspended in fresh DM with 10ng/ml PDGF-BB (Sigma). After 5 passages, a panel of smooth muscle cell markers was detected in ES cell-derived SMCs (esSMCs) by FACS, immunofluorescent staining and reverse transcription PCR. esSMCs were continuously cultured in basic differentiation medium[5].

Reverse transcription-PCR. Total RNA was extracted from cells using RNeasy kit (Qiagen, Valencia, CA, USA) according to the manufacturer's instructions. Reverse transcription was performed using an Improm-II™ RT kit (Promega, Madison, WI, USA). 50ng of cDNA were used in a PCR kit (Invitrogen, San Diego, California, USA) following the manufacturer's instructions. Oligonucleotide primer sequences were as follows: smooth muscle alpha-actin (SMA): F 5'-ACG GCC GCC TCC TCT TCC TC-3', R 5'-GCC CAG CTT CGT CGT ATT CC-3'; smooth muscle protein 22 (SM22): F 5'-GCA GTC CAA AAT TGA GAA GA-3', R 5'-CTG TTG CTG CCC ATT TGA AG-3'; smooth muscle myosin heavy chain (SMMHC): F 5'-ATC TTC TAC TAC CTG CTC GC-3', R 5'-CGG CTG AGA ATC CAT CGG AA-3'; h1-calponin (CAL): F 5'-TAA CCG

AGG TCC TGC CTA CG-3', R 5'-TGT GGG TGG GCT CAC TCA GC-3'; glyceraldehyde-3-phosphate dehydrogenase (GAPDH): F 5'-CGG AGT CAA CGG ATT TGG TCG TAT-3', R 5'-AGC CTT CTC CAT GGT GGT GAA GAC-3'. Stromal-derived factor 1 alpha (SDF1alpha): F 5'- CTT CAT CCC CAT TCT CCT CA-3', R 5' GAC TCT GCT CTG GTG GAA GG-3', IGFBP2: F 5'- GGT GCC AAA CAC CTC AGT CT, R 5'- GGT ATT GGG GTT CAC ACA CC, IGFBP3: F 5'- AAG TTC CAT CCA CTC CAT GC-3', R 5'- AGC TCT GCT TTC TGC CTT TG-3', IGFBP4: F 5'-AGA GCG AAC ATC CCA ACA AC-3', R 5'- ACA GTT TGG AAT GGG GAT GA-3', IGFBP6: F 5'- CAG AGA CCG GCA GAA GAA TC-3', R 5'- CAT CTG GAG ACA CTG GAC AA-3', IGFBP7: F 5'- CAA GAA CAT CTG GAA CGT CA-3', R 5'- TGC GTG GCA CTC ATA CTC TC-3', ApoE: F 5'- GTG CTG TTG GTC ACA TTG CT-3', R 5'- TGT GTG ACT TGG GAG CTC TG-3', Actin: F 5'- CTT CAT CCC CAT TCT CCT CA-3', R 5'- GAC TCT GCT CTG GTG GAA GG-3'.

Proteomic analysis. For proteomics, cell monolayers were rinsed thoroughly with cold PBS to remove any serum components. Protein extracts were prepared from aortic SMCs and esSMCs using a lysis buffer (8M urea, 4% w/v CHAPS, 30mM Tris-Cl, pH 8.5) compatible with DIGE labelling (GE healthcare). After centrifugation at 13,000 g for 10 min, the supernatant containing soluble proteins was harvested and the protein concentration was determined using a modification of the method described by Bradford [6]. The fluorescence dye labelling reaction was carried out at a dye/protein ratio of 400pmol/100μg. After incubation on ice for 30 min, the labelling reaction was stopped by scavenging non-bound dyes with 10mM lysine (L8662, Sigma) for 15 min. For two-dimensional gel electrophoresis, samples were mixed with 2x buffer (8M urea, 4% w/v

CHAPS, 2% w/v DTT, 2% v/v Pharmalytes 3-10 for IEF), 50μg per sample were diluted in rehydration solution (8M urea, 0.5% w/v CHAPS, 0.2% w/v DTT, and 0.2% v/v Pharmalyte pH 3-10) and loaded on IPG strips (18cm, pH 3-10, nonlinear, GE healthcare). After rehydration overnight, strips were focused at 0.05 mA/IPG strip for 60 kVh at 20°C (Multiphor II, GE healthcare). Once IEF was complete the strips were equilibrated in 6M urea containing 30% v/v glycerol, 2% w/v SDS and 0.01% w/v Bromphenol blue, with addition of 1% w/v DTT for 15 min, followed by the same buffer without DTT, but with the addition of 4.8% w/v iodoacetamide for 15 min. SDS-PAGE was performed using 12% T (total acrylamide concentration), 2.6% C (degree of cross-linking) polyacrylamide gels without a stacking gel, using the Ettan DALT system (GE healthcare). The second dimension was terminated when the Bromophenol blue dye front had migrated off the lower end to the gels. After electrophoresis, fluorescence images were acquired using the Typhoon variable mode imager 9400 (GE healthcare). Finally, gels were fixed overnight in methanol: acetic acid: water solution (4:1:5 v/v/v). Protein profiles were visualised by silver staining using the Plus one silver staining kit (GE healthcare) with slight modifications[7] to ensure compatibility with subsequent mass spectrometry analysis. For documentation, silver-stained gels were scanned in transmission scan mode using a calibrated scanner (GS-800, Bio-Rad). Match matrices were created by using Proteomeweaver 2.0 (Definiens). DIGE gels were analysed using the Decyder software (Version 6.5, GE healthcare). For the present study, 18 DIGE gels were processed in parallel to guarantee a maximum of comparability. Each 2-DE run was at least repeated once. All 2-DE gels were of high quality in terms of resolution as well as consistency in spot patterns. Spots exhibiting a statistical difference ($p<0.05$) were

excised for identification. A detailed methodology is available on our website http://www.vascular-proteomics.com.

Tandem Mass Spectrometry. In-gel digestion with trypsin was performed according to published methods[8] modified for use with an Investigator ProGest (Genomic Solutions) robotic digestion system. Following enzymatic degradation, peptides were separated by capillary liquid chromatography on a reverse-phase column (BioBasic-18, 100 x 0.18 mm, particle size 5μm, Thermo Electron Corporation) and applied to a LCQ ion-trap mass spectrometer (LCQ Deca XP Plus, Thermo Electron Corporation). Spectra were collected from the ion-trap mass analyzer using full ion scan mode over the mass-to-charge (m/z) range 300-1800. MS-MS scans were performed on each ion using dynamic exclusion. Database searches were performed using the TurboSEQUEST software (Bioworks Browser version 3.2, Thermo Electron Corporation) against UniProt database. Following filter was applied: for charge state 1, $X_{Corr} > 1.5$; for charge state 2, $X_{Corr} > 2.0$; for charge state 3, $X_{Corr} > 2.5$.

Ingenuity Pathway Analysis (IPA). Differentially expressed proteins were analyzed using Ingenuity Pathway Knowledge Base (Ingenuity System, Mountain View, CA) to determine their most relevant interaction networks and biological functions. The IPA algorithm proceeds by selecting the most connected protein and adding other interconnected proteins to the network. Datasets containing protein accession numbers, fold change and p-values were uploaded into the program application for the analysis. The program generates networks of these proteins using the right-tailed Fisher's Exact Test, by comparing the number of proteins that participate in a given function, relative to the total number of occurrences of those proteins in all functional annotations stored in

the Ingenuity Pathways Knowledge Base, and are then ranked by score, i.e. score of 2 or higher have a 99.9% confidence level of not being randomly assembled into a network. This score was used as the cut-off for identifying protein networks or pathways.

Western blotting. Cellular protein extracts were harvested according to an established protocol. Immunoblotting was performed as described previously[9,10]. The following antibodies were used: pyruvate kinase (7894-9988, Biogenesis, 1:100), lactate dehydrogenase (ab7639-1, 1:100, Abcam), peroxiredoxin-SO_3 (LF-PA0004, 1:2000, Lab Frontier), peroxiredoxin 2 (LF-PA0007, 1:2000, Lab Frontier), peroxiredoxin 3 (LF-PA0030, 1:2000, Lab Frontier), IGFBP3 (R&D, 0.1 μg/ml, AF775), IGFBP6 (R&D, 0.1 μg/ml, AF776).

Cell viability. Cells were cultured on 96-well plates. After 48 hours, cells were incubated with different concentrations of diethyl maleate (DEM, D97703, Sigma) or glucose oxidase (Sigma) for 24 hours. CellTiter 96® AQ_{ueous} One Solution (Cell Proliferation Assay, Promega) was added with dilution ratio of 1:6 in DMEM. After 3 hours incubation, the optical density at 490nm was recorded using photometer[11].

Enzymatic assays. Cells were subject to normoxia or hypoxia in the presence of 5mM, 15mM, and 25mM glucose. After 24h, the remaining glucose in the culture medium was quantified by using glucoseoxidase. Lactate dehydrogenase activity was measured using a commercial assay (CytoTox96, Promega) and following the manufacturer's instruction.

RNase Protection Assay (RPA). Total RNA was extracted using the Qiagen kit according to the manufacturer's instructions. Rnase Protection Assay was performed, using mCK2b, mCR4 and mCK5c multi probe template sets (RiboQuant, Pharmingen,

San Diego, CA) and [α-^{32}P] UTP (Amersham Biosciences) according to the manufacturer's recommendations. The "RNase-protected" fragments were purified and resolved on a 5% sequencing gel and autoradiographed. For quantification, signals for each sample of the blot were normalized to the housekeeping gene L32.

Cytokine measurements. Interleukin-6 and TNF-alpha were measured in the conditioned cell culture medium using commercially available assays (LMC0061 and LMC3011, Biosource) and performed on a Luminex® automated analyser.

Proton nuclear magnetic resonance spectroscopy (NMR). Cellular metabolites were extracted in 6% perchloric acid after rinsing the cells with cold saline[12]. Neutralised extracts were freeze-dried and reconstituted in D_2O. 0.5ml of the extracts were placed in 5mm NMR tubes. ^{1}H NMR spectra were obtained using a Bruker 500MHz spectrometer. The water resonance was suppressed by using gated irradiation centred on the water frequency. 50μl of 5mM sodium 3-trimethylsilyl-2,2,3,3-tetradeuteropropionate (TSP) in D_2O was added to the samples for chemical shift calibration and quantification. Immediately before the NMR analysis, the pH was readjusted to 7 with perchloric acid or KOH.

siRNA knockdown. The siRNA for control and mouse apoE were purchased from Santa Cruz Biotechnology. siRNA experiments were performed using Oligofectamine (Invitrogen) according to the company's recommendations. In brief, SMCs were plated on gelatin-coated 6 well plates and 24h later, siRNA oligonucleotides were introduced into the cells with Oligofectamine in OptiMEM in the absence of serum. The following morning fresh complete medium was added to the cells and the transfected

cells were further cultured for 72h. Protein and RNA samples were subsequently harvested and analysed by Western blot analysis and RT-PCR respectively.

Statistical analysis. Statistical analysis was performed using the analysis of variance and Student's *t*-test. Pairwise comparisons between metabolites were performed using the Bonferroni / Dunn test. Results were given as means±SE. A P value <0.05 was considered significant. For proteomic datasets, DIGE gels were analysed using the EDA module of the Decyder software (GE healthcare). Principal component analysis (PCA) was performed on all differentially expressed proteins after removal of missing values to give an initial overview of the groupings. For pattern analysis, hierarchical clustering was performed on the Student's T-test<0.05 dataset to visualize if replica spot maps are clustered together and to view the general protein patterns in the data set.

References

1. Hu Y, Zou Y, Dietrich H, Wick G, Xu Q. Inhibition of neointima hyperplasia of mouse vein grafts by locally applied suramin. *Circulation*. 1999;100:861-8.
2. Xu Q, Li DG, Holbrook NJ, Udelsman R. Acute hypertension induces heat-shock protein 70 gene expression in rat aorta. *Circulation*. 1995;92:1223-9.
3. Hu Y, Zhang Z, Torsney E, Afzal AR, Davison F, Metzler B, Xu Q. Abundant progenitor cells in the adventitia contribute to atherosclerosis of vein grafts in ApoE-deficient mice. *J Clin Invest*. 2004;113:1258-65.
4. Vittet D, Prandini MH, Berthier R, Schweitzer A, Martin-Sisteron H, Uzan G, Dejana E. Embryonic stem cells differentiate in vitro to endothelial cells through successive maturation steps. *Blood*. 1996;88:3424-31.
5. Yin X, Mayr M, Xiao Q, Wang W, Xu Q. Proteomic analysis reveals higher demand for antioxidant protection in embryonic stem cell-derived smooth muscle cells. *Proteomics*. 2006;6:6437-6446.
6. Bradford MM. A rapid and sensitive method for the quantitation of microgram quantities of protein utilizing the principle of protein-dye binding. *Anal Biochem*. 1976;72:248-54.
7. Yan JX, Wait R, Berkelman T, Harry RA, Westbrook JA, Wheeler CH, Dunn MJ. A modified silver staining protocol for visualization of proteins compatible with matrix-assisted laser desorption/ionization and electrospray ionization-mass spectrometry. *Electrophoresis*. 2000;21:3666-72.
8. Shevchenko A, Wilm M, Vorm O, Mann M. Mass spectrometric sequencing of proteins silver-stained polyacrylamide gels. *Anal Chem*. 1996;68:850-8.
9. Li C, Hu Y, Mayr M, Xu Q. Cyclic strain stress-induced mitogen-activated protein kinase (MAPK) phosphatase 1 expression in vascular smooth muscle cells is regulated by Ras/Rac-MAPK pathways. *J Biol Chem*. 1999;274:25273-80.
10. Li C, Hu Y, Sturm G, Wick G, Xu Q. Ras/Rac-Dependent activation of p38 mitogen-activated protein kinases in smooth muscle cells stimulated by cyclic strain stress. *Arterioscler Thromb Vasc Biol*. 2000;20:E1-9.
11. Mayr U, Mayr M, Li C, Wernig F, Dietrich H, Hu Y, Xu Q. Loss of p53 accelerates neointimal lesions of vein bypass grafts in mice. *Circ Res*. 2002;90:197-204.
12. Bergmeyer H. *Methods of enzymatic analysis*. Weinheim, Germany: Verlag Chemie; 1974.

SUPPLEMENT

Supplement Figure I. Differentially expressed proteins in normoxic apoE$^{-/-}$ SMCs. Protein extracts from normoxic apoE$^{+/+}$ and apoE$^{-/-}$ SMCs were separated by two-dimensional electrophoresis and quantified using the difference-in gel electrophoresis approach (DIGE). Differentially expressed spots are numbered and were identified by tandem mass spectrometry (supplemental Table I).

Supplement Figure II. Pathway analysis for apoE$^{-/-}$ SMCs. 41 proteins formed components of three individual pathway groups. 20 were grouped in a dominant network with a score of 47 (A). The 2 minor groups with a score of 19 and 32 were merged. Glucose constituted a core of this protein association network (B). The orange lines indicate the edges added during the merging of the two networks. Red and green colors indicate up- and downregulation of protein isoforms, respectively (supplemental Table I).

Supplement Figure III. Differentially expressed proteins in hypoxic SMCs.

Protein extracts from hypoxic apoE$^{+/+}$ and apoE$^{-/-}$ SMCs were separated by two-dimensional electrophoresis and compared to normoxic controls using the difference-in gel electrophoresis approach (DIGE). Differentially expressed spots are numbered and were identified by tandem mass spectrometry (supplemental Table II).

Supplement Figure IV. Alterations of enzymatic pathways in hypoxic SMCs. Hypoxia-induced enzymatic changes as identified by proteomics are displayed in the context of metabolic pathways (**K**yoto **E**ncyclopedia of **G**enes and **G**enomes, http://

www.genome.jp/kegg/). Red and green colors indicate up- and downregulation in hypoxic SMCs, respectively.

Supplement Figure V. Differentially expressed proteins in hypoxic apoE$^{-/-}$ SMCs.

Protein extracts from hypoxic apoE$^{-/-}$ SMCs were separated by two-dimensional electrophoresis and compared to hypoxic apoE$^{+/+}$ SMCs using the difference-in gel electrophoresis approach (DIGE). Differentially expressed spots are numbered and were identified by tandem mass spectrometry (supplemental Table III).

Supplement Figure VI. Comparison of metabolites in the conditioned medium.

Metabolite concentrations in the conditioned medium of hypoxic apoE$^{+/+}$ (white) and apoE$^{-/-}$ (black) SMCs as determined by high-resolution NMR spectroscopy. Note that the depletion of glucose and accumulation of acetate was faster in the culture medium of apoE$^{-/-}$ SMCs compared to apoE$^{+/+}$ controls.

Supplement Table I. Differentially expressed proteins in normoxic apoE$^{-/-}$ compared to apoE$^{+/+}$ SMCs.

N	Protein identity	SWISS PROT Accession No.	Calculated pI/ MM Da (x10^3)	No. of peptides	Coverage (%)	Ratio*	p
	Glucose metabolism						
37	Pyruvate dehydrogenase E1 component alpha	ODPA_MOUSE	8.49 / 43.23	2	5.64	1.22	0.032
43	L-lactate dehydrogenase A chain	LDHA_MOUSE	7.76 / 36.67	13	37.46	1.23	0.0028
44	Glyceraldehyde-3-phosphate dehydrogenase	G3P_MOUSE	8.45 / 35.68	6	22.89	1.51	0.0025
	Energy metabolism						
50	Voltage-dependent anion-selective channel protein	VDAC1_MOUSE	8.55 / 32.35	6	21.62	2.34	0.00024
51	Voltage-dependent anion-selective channel protein	VDAC1_MOUSE	8.55 / 32.35	17	80.41	1.26	0.011
	Lipid metabolism						
22	Propionyl-CoA carboxylase alpha chain, mitochondrial	PCCA_MOUSE	6.83 / 79.92	2	3.73	-1.55	0.0035
36	Acyl-CoA dehydrogenase, mitochondrial	ACADL_MOUSE	8.53 / 47.91	6	13.72	1.23	0.031
47	3-Hydroxyisobutyrate dehydrogenase, mitochondrial	3HIDH_MOUSE	8.37 / 35.44	2	8.66	1.55	0.044
	Amino Acid metabolism						
20	Procollagen-lysine,2-oxoglutarate 5-dioxygenase 2	PLOD2_MOUSE	6.34 / 84.53	23	31.48	-1.61	0.0074
33	Ornithine aminotransferase, mitochondrial	OAT_MOUSE	6.19 / 48.36	6	13.90	-1.40	0.032
30	Glutamate dehydrogenase 1, mitochondrial	DHE3_MOUSE	8.05 / 61.34	12	26.16	-1.31	0.0035
46	Pyrroline-5-carboxylate reductase 1	P5CR1_MOUSE	6.40 / 32.40	2	7.77	-1.38	0.0057
	Calcium-binding proteins						
4	Reticulocalbin-3	RCN3_MOUSE	4.74 / 38.00	3	10.67	-1.49	0.0021
5	Calumenin (Crocalbin)	CALU_MOUSE	4.49 / 37.06	8	24.44	-1.44	0.018
6	Calreticulin	CRTC_MOUSE	4.33 / 48.00	15	33.89	1.54	0.042
26	Caldesmon 1	Q8VCQ8_MOUSE	6.98 / 60.45	18	28.87	-1.92	0.00080
	Cytoskeleton/Myofilaments /Intermediate filaments						
1	Tropomyosin 1 alpha chain	TPM1_MOUSE	4.69 / 32.68	20	58.80	-1.58	0.02
12	Lamin B1	LAM1_MOUSE	5.11 / 66.66	16	30.32	1.45	0.017

24	Lamin A	LAMA_MOUSE	6.54 / 74.21	4	4.51	-2.02	0.0011
	Cytoskeletal regulators						
3	Annexin A5	ANXA5_MOUSE	4.83 / 35.75	7	20.69	-1.78	0.00096
18	Ezrin (p81)	EZRI_MOUSE	5.80 / 69.30	6	10.60	2.18	0.032
19	Ezrin (p81)	EZRI_MOUSE	5.80 / 69.30	15	17.09	3.08	0.046
23	Radixin	RADI_MOUSE	5.85 / 68.60	2	3.95	1.60	0.0025
25	Moesin	MOES_MOUSE	6.24 / 37.64	12	18.06	-2.01	0.00077
31	Fascin (Singed-like-protein)	FSCN1_MOUSE	6.20 / 54.30	18	43.70	1.87	7.5e-005
32	Fascin (Singed-like-protein)	FSCN1_MOUSE	6.20 / 54.30	1	2.64	1.34	4.8e-005
39	Annexin A2	ANXA2_MOUSE	7.53 / 38.55	12	37.87	1.53	6.9e-006
40	Annexin A2	ANXA2_MOUSE	7.50 / 38.50	11	35.21	1.32	0.016
41	Annexin A2	ANXA2_MOUSE	7.50 / 38.50	18	57.99	1.50	0.00016
42	Annexin A2	ANXA2_MOUSE	7.50 / 38.50	16	48.22	1.67	2.7e-008
45	PDZ and LIM domain protein 1	PDLI1_MOUSE	6.37 / 35.59	2	6.46	1.39	0.024
	ER proteins						
8	Endoplasmin	ENPL_MOUSE	4.74 / 92.48	23	28.93	1.65	0.0025
10	Endoplasmin	ENPL_MOUSE	4.74 / 92.48	10	9.35	1.67	0.0024
11	78 kDa glucose-regulated protein	GRP78_MOUSE	5.07 / 72.42	17	36.18	1.94	0.0036
14	Protein disulfide-isomerase A3	PDIA3_MOUSE	5.99 / 56.62	12	22.02	1.42	0.0028
15	Protein disulfide-isomerase A3	PDIA3_MOUSE	5.99 / 56.62	18	47.62	1.53	0.00035
16	Protein disulfide-isomerase A3	PDIA3_MOUSE	5.99 / 56.62	11	21.83	1.42	0.023
34	Protein disulfide-isomerase A6	PDIA6_MOUSE	5.00 / 48.10	5	16.59	1.24	0.034
35	Protein disulfide-isomerase A6	PDIA6_MOUSE	5.00 / 48.10	5	20.23	1.57	0.0089
49	Endoplasmic reticulum protein Erp29	ERP29_MOUSE	5.90 / 28.80	4	17.56	1.43	9.6e-006
	Protein folding						
17	Stress-70 protein, mitochondrial	GRP75_MOUSE	5.91 / 73.53	24	45.51	1.77	0.0065
29	T-complex protein 1 subunit delta	TCPD_MOUSE	8.33 / 57.94	17	29.18	1.33	0.016
38	40 kDa peptidyl-prolyl cis-trans isomerase	PPID_MOUSE	7.10 / 40.10	4	11.92	1.37	0.021
	Transcription / translation						
2	Elongation factor 1 -delta	EF1D_MOUSE	4.91 / 31.16	2	8.93	-1.45	0.023

13	Heterogeneous nuclear ribonucleoprotein K	HNRPK_MOUSE	5.39 / 50.98	10	28.51	1.21	0.011
21	Elongation factor 2	EF2_MOUSE	6.42 / 95.78	5	6.18	-1.28	0.0030
27	Far upstream element-binding protein 1	FUBP1_MOUSE	7.73 / 68.54	5	9.98	1.27	0.025
	Proteolysis						
48	Proteasome subunit alpha type 1	PSA1_MOUSE	6.00 / 29.55	5	21.29	1.35	2.8e-005
	Others						
7	Hypoxia up-regulated 1	Q80X75_MOUSE	5.20 / 111.12	8	8.51	1.28	0.023
9	Vascular cell adhesion protein 1	VCAM1_MOUSE	5.21 / 81.32	2	3.65	-1.61	0.00013
28	Programmed cell death protein 8, mitochondrial	PDCD8_MOUSE	9.23 / 66.77	7	14.87	1.26	0.016
52	ELAV-like protein 1	ELAV1_MOUSE	9.23 / 36.07	8	13.50	-1.20	0.030

* A negative or positive ratio indicates a decrease or an increase in apoE$^{-/-}$ SMCs compared to wildtype controls, respectively. P-values are derived from t-tests.

Supplement Table II. Differentially expressed proteins in hypoxic compared to normoxic SMCs.

N	Protein identity	SWISS PROT Accession No.	Calculated pI/ MM Da (x10^3)	No. of peptides	Coverage (%)	Ratio*	p
	Glucose metabolism						
14	Pyruvate kinase, M2	KPYM_MOUSE	7.42 / 57.76	12	19.43	1.22	0.0077
19	Alpha-enolase	ENOA_MOUSE	6.36 / 47.01	22	44.11	1.47	0.039
21	Alpha-enolase	ENOA_MOUSE	6.36 / 47.01	31	57.74	1.54	0.045
22	Alpha-enolase	ENOA_MOUSE	6.36 / 47.01	24	63.97	1.59	0.026
29	Phosphoglycerate kinase 1	PGK1_MOUSE	7.52 / 44.41	4	12.02	1.22	0.016
30	L-lactate dehydrogenase A chain	LDHA_MOUSE	7.61 / 36.50	13	33.43	1.42	0.0018
34	Triosephosphate isomerase	TPIS_MOUSE	7.09 / 26.58	5	23.79	1.38	0.044
35	Triosephosphate isomerase	TPIS_MOUSE	7.09 / 26.58	6	28.23	1.88	2.80e-04
	Pyruvate Dehydrogenase Complex						
15	Dihydrolipoyl dehydrogenase	DLDH_MOUSE	7.97 / 54.21	16	25.54	-1.24	0.0092
16	Dihydrolipoyl dehydrogenase	DLDH_MOUSE	7.97 / 54.21	4	9.04	-1.42	0.00073
25	Pyruvate dehydrogenase E1 component alpha subunit	ODPA_MOUSE	8.49 / 43.23	3	8.46	-2.16	0.00011
	Energy metabolism						
31	Vacuolar ATP synthase subunit E	VATE_MOUSE	9.28 / 26.59	2	9.21	-1.39	0.0046
33	Adenylate kinase isoenzyme 2	KAD2_MOUSE	7.16 / 25.48	1	4.76	1.99	1.30e-05
37	Electron transfer flavoprotein beta-subunit	ETFB_MOUSE	8.56 / 27.31	4	19.84	-1.29	8.50e-03
38	GTP:AMP phosphotransferase	KAD3_MOUSE	8.87 / 25.43	3	17.62	-1.32	0.0022
	Citric acid cycle						
8	Aconitate hydratase	ACON_MOUSE	8.08 / 85.46	14	20.90	-1.26	0.0092
9	Aconitate hydratase	ACON_MOUSE	8.08 / 85.46	9	13.72	-1.27	0.012
10	Aconitate hydratase	ACON_MOUSE	8.08 / 85.46	9	13.72	-1.28	0.008
11	Aconitate hydratase	ACON_MOUSE	8.08 / 85.46	25	33.08	-1.24	0.028
26	Fumarate hydratase	FUMH_MOUSE	9.12 / 54.37	3	9.27	-1.21	0.021
27	Fumarate hydratase	FUMH_MOUSE	9.12 / 54.37	4	10.85	-1.22	0.034

	Lipid metabolism						
20	Aldehyde dehydrogenase	DHAM_MOUSE	7.53 / 56.54	21	44.89	-1.29	0.035
36	Enoyl-CoA hydratase	ECHM_MOUSE	8.76 / 31.48	7	30.00	-1.33	0.028
	Cytoskeleton/Myofilaments /Intermediate filaments						
2	Vimentin	VIME_MOUSE	5.06 / 53.69	34	57.94	1.23	0.024
4	Vimentin	VIME_MOUSE	5.06 / 53.69	42	78.76	1.21	0.038
5	Vimentin	VIME_MOUSE	5.06 / 53.69	34	57.30	1.23	0.019
6	Vimentin	VIME_MOUSE	5.06 / 53.69	47	77.90	1.30	0.028
	Protein folding						
13	T-complex protein 1, delta subunit	TCPD_MOUSE	8.33 / 57.94	4	8.74	1.20	0.023
17	T-complex protein 1, alpha subunit	TCP1_MOUSE	5.76 / 60.34	2	5.94	1.30	0.011
	Transcription / translation						
7	Heterogeneous nuclear ribonucleoprotein K	HNRPK_MOUSE	5.39 / 50.98	6	15.12	-1.21	0.006
12	Far upstream element binding protein 1	FUBP1_MOUSE	7.73 / 68.54	8	13.36	1.20	0.048
28	Splicing factor 3b, subunit 4	Q8QZY9_MOUSE	8.55 / 44.36	1	3.30	1.32	0.0084
	Antioxidants						
3	Thioredoxin domain containing protein 5	TXND5_MOUSE	5.51 / 46.42	11	23.02	-1.26	0.0099
32	Gluthione transferase omega 1	GSTO1_MOUSE	6.91 / 27.50	5	18.75	1.32	0.025
	Others						
1	Reticulocalbin-1	RCN1_MOUSE	4.70 / 38.11	7	23.38	-1.34	0.0079
18	Nucleoporin 50kDa	NUP50_MOUSE	5.94 / 49.50	4	7.73	1.24	0.001
23	Flotillin-1	FLOT1_MOUSE	6.71 / 47.51	7	16.12	-1.21	0.022
24	Argininosuccinate lyase	ARLY_MOUSE	6.48 / 51.74	1	1.29	-1.39	0.0006

* A negative or positive ratio indicates a decrease or an increase in hypoxic $apoE^{+/+}$ and $apoE^{-/-}$ SMCs compared to normoxic controls, respectively. P-values are derived from t-tests.

Supplement Table III. Differentially expressed proteins in hypoxic apoE$^{-/-}$ compared to apoE$^{+/+}$ SMCs.

N	Protein identity	SWISS PROT Accession No.	Calculated pI/ MM Da (x10^3)	No. of peptides	Coverage (%)	Ratio*	p
	Glucose metabolism						
29	Pyruvate kinase, isozyme M2	KPYM_MOUSE	7.42 / 57.76	9	19.81	1.47	0.01
32	Glucose-6-phosphate 1-dehydrogenase X	G6PD1_MOUSE	6.07 / 59.13	8	16.54	1.73	0.0057
42	Pyruvate dehydrogenase E1 component alpha subunit	ODPA_MOUSE	8.49 / 43.23	10	24.87	1.75	0.0026
50	Transaldolase	TALDO_MOUSE	6.57 / 37.39	2	7.42	2.01	0.0067
52	Aldose reductase	ALDR_MOUSE	6.79 / 35.60	15	34.29	1.51	0.042
	Electron transport and oxidative phosphorylation						
38	ATP synthase alpha chain, mitochondrial	ATPA_MOUSE	9.22 / 59.75	14	26.04	1.75	0.012
39	ATP synthase alpha chain, mitochondrial	ATPA_MOUSE	9.22 / 59.75	18	31.83	1.82	0.036
61	Vacuolar ATP synthase subunit E	VATE1_MOUSE	9.28 / 26.59	2	9.21	1.45	0.0061
	Malate-Aspartate Shuttle						
45	Aspartate aminotransferase, cytoplasmic	AATC_MOUSE	6.75 / 46.10	10	26.70	1.63	0.043
60	Malate dehydrogenase	MDHC_MOUSE	6.16 / 36.47	4	13.77	1.87	0.0037
	Lipid metabolism						
44	Acyl coenzyme A thioester hydrolase 2, mitochondrial	AC48_MOUSE	8.74 / 50.56	1	2.28	1.31	0.021
53	Alcohol dehydrogenase	AKA1_MOUSE	6.90 / 36.59	6	14.46	2.11	0.0030
63	Enoyl-CoA hydratase, mitochondrial	ECHM_MOUSE	8.76 / 31.48	4	18.62	1.52	0.0012
	Amino acid metabolism						
18	Delta 1-pyrroline-5-carboxylate synthetase	P5CS_MOUSE	7.18 / 87.30	5	5.91	-1.48	0.0099
40	Serine hydroxymethyl transferase 2, mitochondrial	Q99K87_MOUSE	8.72 / 55.76	19	40.87	-2.03	0.028
43	Argininosuccinate lyase	ARLY_MOUSE	6.48 / 51.74	1	1.29	1.25	0.026
58	Pyrroline-5-carboxylate reductase 1	P5CR1_MOUSE	6.36 / 32.37	2	7.77	-1.23	0.0019
	Calcium-binding proteins						
22	Caldesmon 1	Q8VCQ_MOUSE	6.98 / 60.45	21	33.02	-1.97	0.036

	Cytoskeleton/Myofilaments /Intermediate filaments						
8	Vimentin	VIME_MOUSE	5.06 / 53.56	14	32.47	-1.55	0.00069
9	Vimentin	VIME_MOUSE	5.06 / 53.56	20	35.05	-1.29	0.022
10	Vimentin	VIME_MOUSE	5.06 / 53.56	38	78.76	-1.34	0.0037
11	Vimentin	VIME_MOUSE	5.06 / 53.56	34	57.30	-1.26	0.034
12	Vimentin	VIME_MOUSE	5.06 / 53.56	47	77.90	-1.51	0.0029
19	Lamin A	LAMA_MOUSE	6.54 / 74.21	12	18.35	-1.53	0.00067
20	Lamin A	LAMA_MOUSE	6.54 / 74.21	25	35.49	-1.39	0.0054
21	Lamin A	LAMA_MOUSE	6.54 / 74.21	25	35.49	-1.41	0.0066
	Cytoskeletal regulators						
5	F-actin capping protein beta subunit	CAPZB_MOUSE	5.47 / 31.22	4	14.13	1.33	0.023
16	Ezrin p81 Cytovillin (Villin-2)	EZRI_MOUSE	5.83 / 69.28	6	10.60	3.53	8.9e-07
17	Ezrin p81 Cytovillin (Villin 2)	EZRI_MOUSE	5.83 / 69.28	15	17.09	5.33	9.00e-05
36	Fascin (Singed-like protein)	FSCN1_MOUSE	6.21 / 54.27	2	2.64	1.56	0.018
37	Fascin (Singed-like protein)	FSCN1_MOUSE	6.21 / 54.27	18	43.70	1.98	0.017
51	Annexin A1 (Lipocortin I)	ANXA1_MOUSE	7.15 / 38.60	19	65.22	2.81	0.032
55	Annexin A2 (Lipocortin II)	ANXA2_MOUSE	7.53 / 38.54	12	35.21	1.32	0.041
56	Annexin A2 (Lipocortin II)	ANXA2_MOUSE	7.53 / 38.54	19	57.99	1.41	0.025
57	Annexin A2 (Lipocortin II)	ANXA2_MOUSE	7.53 / 38.54	18	48.22	1.39	0.028
65	Transgelin	TAGL_MOUSE	8.86 / 22.45	4	20.50	4.34	0.035
	ER proteins						
2	Protein disulfide-isomerase (fragment)	PDIA1_MOUSE	4.79 / 57.14	6	11.39	1.21	0.047
3	Protein disulfide-isomerase (fragment)	PDIA1_MOUSE	4.79 / 57.14	6	11.39	1.26	0.043
4	Endoplasmic reticulum protein ERp29	ERP29_MOUSE	5.90 / 28.82	4	17.56	1.84	0.0065
49	Protein disulfide-isomerase A6	PDIA6_MOUSE	5.00 / 48.10	1	3.18	1.54	0.035
	Protein folding						
13	Stress-70 protein, mitochondrial	GRP75_MOUSE	5.91 / 73.53	16	27.98	-1.40	0.03
30	T-complex protein 1, zeta subunit	TCPZ_MOUSE	6.67 / 57.87	4	6.60	-1.52	0.038
31	T-complex protein 1, zeta subunit	TCPZ_MOUSE	6.67 / 57.87	9	17.17	-1.45	0.024
41	47 kDa heat shock protein	HSP47_MOUSE	8.90 / 46.59	2	4.80	1.33	0.04
47	40kDa peptidyl-prolyl cis-trans isomerase	PPID_MOUSE	7.06 / 40.61	4	11.92	1.53	0.01

	Transcription / translation						
15	Elongation factor 2	EF2_MOUSE	6.42 / 95.18	11	12.95	-1.26	0.0096
23	Activated spleen cDNA	Q3U0V1_MOUSE	6.90 / 76.81	10	20.45	-1.37	0.0046
24	Activated spleen cDNA	Q3U0V1_MOUSE	6.90 / 76.81	9	18.18	-1.36	0.013
25	Probable RNA-dependent helicase p68	DDX5_MOUSE	9.06 / 69.32	13	21.66	-1.44	0.03
26	Nuclear protein SkiP	SNW1_MOUSE	9.49 / 61.48	6	12.87	-1.48	0.0072
27	Non-POU domain containing octamer-binding protein	NONO_MOUSE	9.01 / 54.54	6	10.57	-1.26	0.019
28	Polypyrimide tract-binding protein 1	PTBP1_MOUSE	8.47 / 56.47	7	16.89	-1.40	0.0068
33	Homolog, Nuclear matrix protein 200	PRP19_MOUSE	6.14 / 55.24	5	13.10	-1.29	0.016
34	Homolog, Nuclear matrix protein 200	PRP19_MOUSE	6.14 / 55.24	11	22.22	-1.27	0.0045
35	Homolog, Nuclear matrix protein 200	PRP19_MOUSE	6.14 / 55.24	2	4.17	-1.23	0.021
46	Heterogeneous nuclear ribonucleoprotein A/B	ROAA_MOUSE	7.69 / 30.83	5	18.60	-1.22	0.027
48	Heterogeneous nuclear ribonucleoprotein A/B	ROAA_MOUSE	7.69 / 30.83	8	24.21	-1.23	0.0051
54	Heterogeneous nuclear ribonucleoprotein A/B	ROAA_MOUSE	7.69 / 30.83	6	23.51	-1.27	0.031
68	GTP-binding nuclear protein	RANT_MOUSE	6.08 / 24.45	4	16.67	1.22	0.0086
	Proteolysis						
59	Proteasome non-ATPase regulatory subunit	PSDE_MOUSE	6.06 / 34.58	2	6.45	1.30	0.016
62	Proteasome subunit alpha type 6	PSA6_MOUSE	6.35 / 27.37	4	17.48	1.34	0.045
69	Proteasome subunit beta type 3	PSB3_MOUSE	6.15 / 22.97	3	20.00	1.31	0.043
	Antioxidants						
66	Peroxiredoxin 1	PRDX1_MOUSE	8.26 / 22.18	6	26.13	2.43	0.0059
67	Peroxiredoxin 1	PRDX1_MOUSE	8.26 / 22.17	5	21.61	1.91	0.017
	Others						
1	Cytochrome b5	CYB5_MOUSE	4.96 / 15.11	2	15.79	1.95	3.00e-05
6	Clathrin light chain A	CLCA_MOUSE	4.45 / 25.56	3	10.21	1.28	0.01
7	SET protein (Phosphatase 2A inhibitor I2PP2A)	SET_MOUSE	4.22 / 33.38	6	24.91	-1.22	0.039
14	Vascular cell adhesion protein 1	VCAM1_MOUSE	5.21 / 81.32	8	11.64	-1.47	0.024

* A negative or positive ratio indicates a decrease or an increase in hypoxic apoE$^{-/-}$ SMCs compared to hypoxic wildtype controls, respectively. P-values are derived from t-tests.

Supplement Table IV. Metabolic effects of glucose concentrations in normoxic apoE$^{+/+}$ and apoE$^{-/-}$ SMCs.

	apoE$^{+/+}$		apoE$^{-/-}$		P
	5mM (n=4)	**25mM** (n=4)	**5mM** (n=5)	**25mM** (n=5)	(ANOVA)
Leucine	25.86 (±3.07)	24.27 (±1.94)	22.65 (±2.26)	31.77 (±3.89)	0.168
Isoleucine	24.37 (±1.35)	22.30 (±2.36)	20.34 (±1.95)	27.57 (±3.17)	0.166
Valine	30.90 (±1.56)	29.01 (±2.99)	29.78 (±3.06)	36.91 (±4.20)	0.292
Lactate	266.71 (±14.67)	267.05 (±28.68)	357.96 (±36.13)	**617.88 (±120.63) ***	**0.004**
Alanine	129.07 (±17.64)	154.21 (±11.41)	122.99 (±26.29)	191.96 (±15.51)	0.055
Acetate	15.86 (±3.85)	11.32 (±2.61)	19.31 (±5.33)	15.34 (±2.15)	0.544
Glutamate	134.61 (±10.60)	138.94 (±10.46)	123.75 (±21.78)	138.30 (±7.69)	0.860
Succinate	19.30 (±2.20)	17.38 (±1.63)	18.10 (±1.97)	21.02 (±0.85)	0.451
Glutamine	49.21 (±9.42)	45.05 (±4.87)	36.59 (±12.11)	47.78 (±4.10)	0.710
Choline	2.50 (±0.359)	2.23 (±0. 28)	1.80 (±0.29)	**3.64 (±061) ***	**0.021**
Phosphocholine	11.32 (±1.55)	**7.01 (±0.79)**	12.28 (±1.35)	9.36 (±1.11)	**0.029**
Carnitine	31.35 (±5.44)	40.93 (±5.32)	**18.68 (±2.45) ***	33.81 (±2.32)	**0.002**
Myoinositol	49.56 (±6.70)	**132.50 (±39.30)**	46.66 (±3.92)	**187.64 (±19.73)**	**< 0.001**
Glucose	21.13 (±7.45)	120.14 (±32.30)	7.98 (±2.88)	403.89 (±227.98)	0.200
Tyrosine	14.72 (±1.94)	15.68 (±0.67)	17.82 (±2.41)	18.84 (±1.58)	0.582
Total Creatine	90.58 (±11.71)	78.23 (±7.77)	76.20 (±13.49)	101.17 (±12.00)	0.246
Adenosine nucleotides	37.85 (±4.63)	41.36 (±2.99)	35.75 (±5.99)	36.79 (±4.35)	0.091
Glycolic acid	31.36 (±10.92)	36.37 (±5.43)	27.55 (±2.85)	34.71 (±2.67)	0.439
Glycine	140.34 (±47.56)	147.38 (±11.54)	147.15 (±32.63)	234.16 (±2.67)	0.131

Data presented are given in μmol/g wet weight (mean±SE), P-values for differences between all groups were derived from ANOVA tables (bold numbers highlight significant differences from controls in the Fisher PSLD test, * significant differences to apoE$^{+/+}$ SMCs)

Supplement Table V. Metabolic effects of glucose concentrations in hypoxic apoE$^{+/+}$ and apoE$^{-/-}$ SMCs

	apoE$^{+/+}$		apoE$^{-/-}$		P
	5mM (n=9)	**25mM** (n=9)	**5mM** (n=9)	**25mM** (n=9)	(ANOVA)
Leucine	10.95 (±1.70)	**26.03 (±2.96)**	9.17 (±1.00)	**20.54 (±2.49)**	<0.001
Isoleucine	10.68 (±1.57)	**24.52 (±3.24)**	8.90 (±0.98)	**20.10 (±2.62)**	<0.001
Valine	12.21 (±1.88)	**28.00 (±3.69)**	10.55 (±1.20)	**22.79 (±2.69)**	<0.001
Lactate	111.74 (±23.58)	**430.29 (±61.88)**	83.48 (±14.58)	**509.58 (±67.82)**	<0.001
Alanine	26.10 (±2.44)	**54.59 (±5.52)**	31.05 (±2.84)	**60.14 (±4.36)**	<0.001
Acetate	7.93 (±2.83)	13.06 (±6.08)	11.58 (±5.73)	7.02 (±1.49)	0.742
Glutamate	57.35 (±4.63)	73.84 (±4.53)	60.96 (±3.89)	60.46 (±5.87)	0.093
Succinate	14.92 (±2.54)	9.95 (±2.65)	11.00 (±2.33)	15.77 (±1.39)	0.215
Glutamine	31.26 (±10.11)	42.37 (±2.48)	20.39 (±6.31)	**48.92 (±3.50)**	0.017
Choline	2.67 (±0.65)	4.10 (±0.74)	3.90 (±1.37)	4.21 (±0.68)	0.611
Phosphocholine	9.40 (±1.90)	11.78 (±3.35)	7.64 (±1.20)	10.86 (±1.68)	0.566
Carnitine	32.41 (±10.17)	49.11 (±12.42)	28.68 (±10.45)	42.94 (±15.79)	0.625
Taurine	68.02 (±6.93)	**204.00 (±43.74)**	54.59 (±2.91)	**183.17 (±33.52)**	<0.001
Glucose	9.75 (±1.27)	**148.97 (±37.87)**	3.63 (±0.61)	**92.05 (±23.41)**	<0.001
Tyrosine	5.36 (±1.66)	12.49 (±0.97)	4.27 (±0.64)	9.72 (±0.95)	<0.001
Total Creatine	25.16 (±1.76)	**55.70 (±14.75)**	28.42 (±3.98)	**58.97 (±9.92)**	0.020
Adenosine nucleotides	7.88 (±1.85)	9.47 (±2.07)	7.28 (±1.59)	12.29 (±2.77)	0.354
Glycolic acid	23.60 (±4.88)	26.57 (±9.55)	**14.03 (±1.36) ***	**40.88 (±4.24) ***	<0.001
Glycine	56.81 (±5.72)	**88.15 (±15.86)**	51.97 (±5.61)	**84.28 (±9.72)**	0.031

See legend to Supplement Table IV.

Supplement Table VI. Co-regulation of apoE, IL-6, and IGFBP expression.

	$ApoE^{-/-}$ SMCs		$ApoE^{+/+}$ SMCs	
	Control	+ IL-6	+ Cholesterol	+ si ApoE
Apo E	N/A	N/A	↓	↓
IL-6	↓	↑	↓	↓
IGFBP-3	↑	↓	↑	-
IGFBP-6	↑	↓	↑	↑

Supplemental Figure I **Mayr et al**

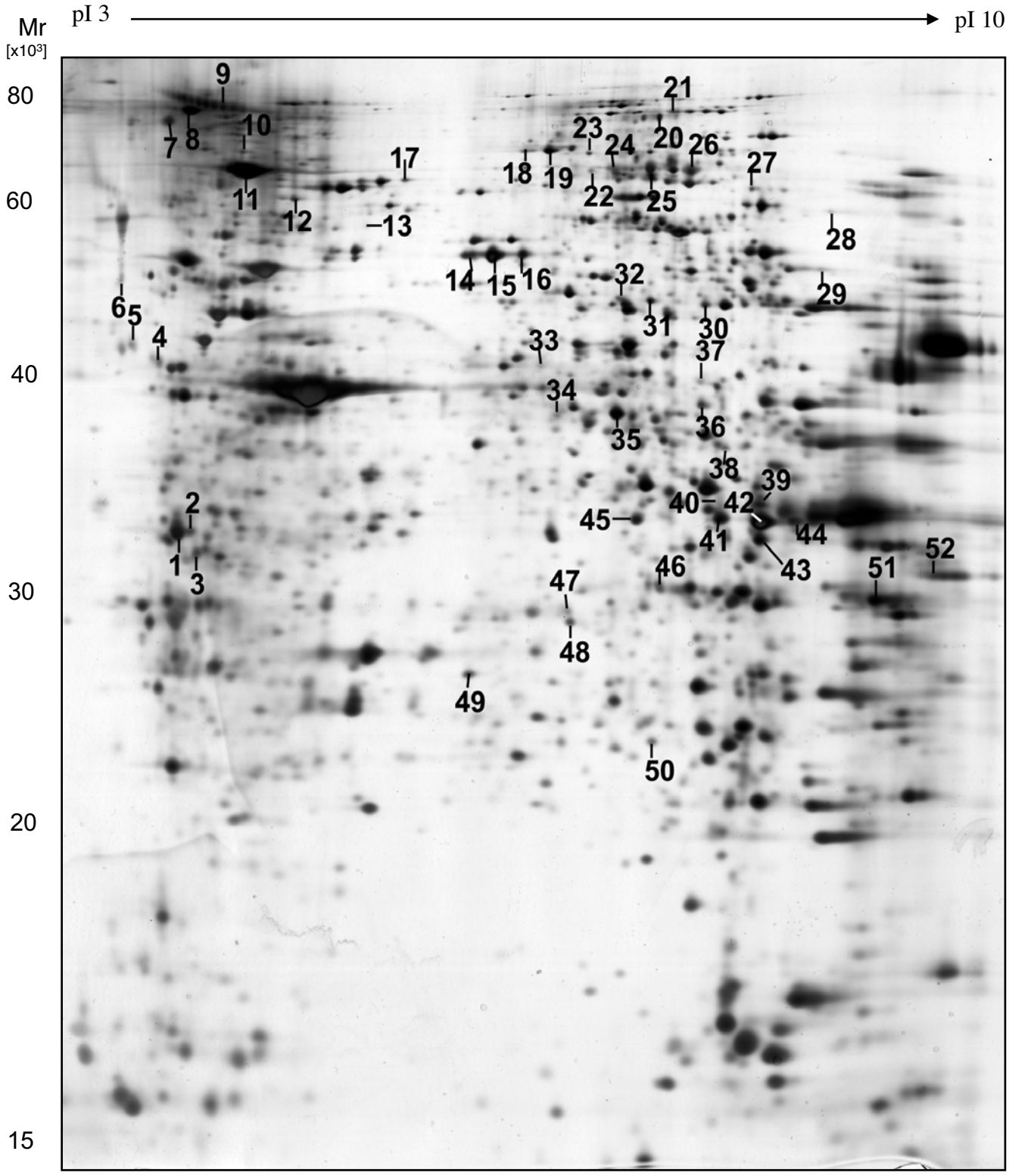

Supplemental Figure II **Mayr et al**

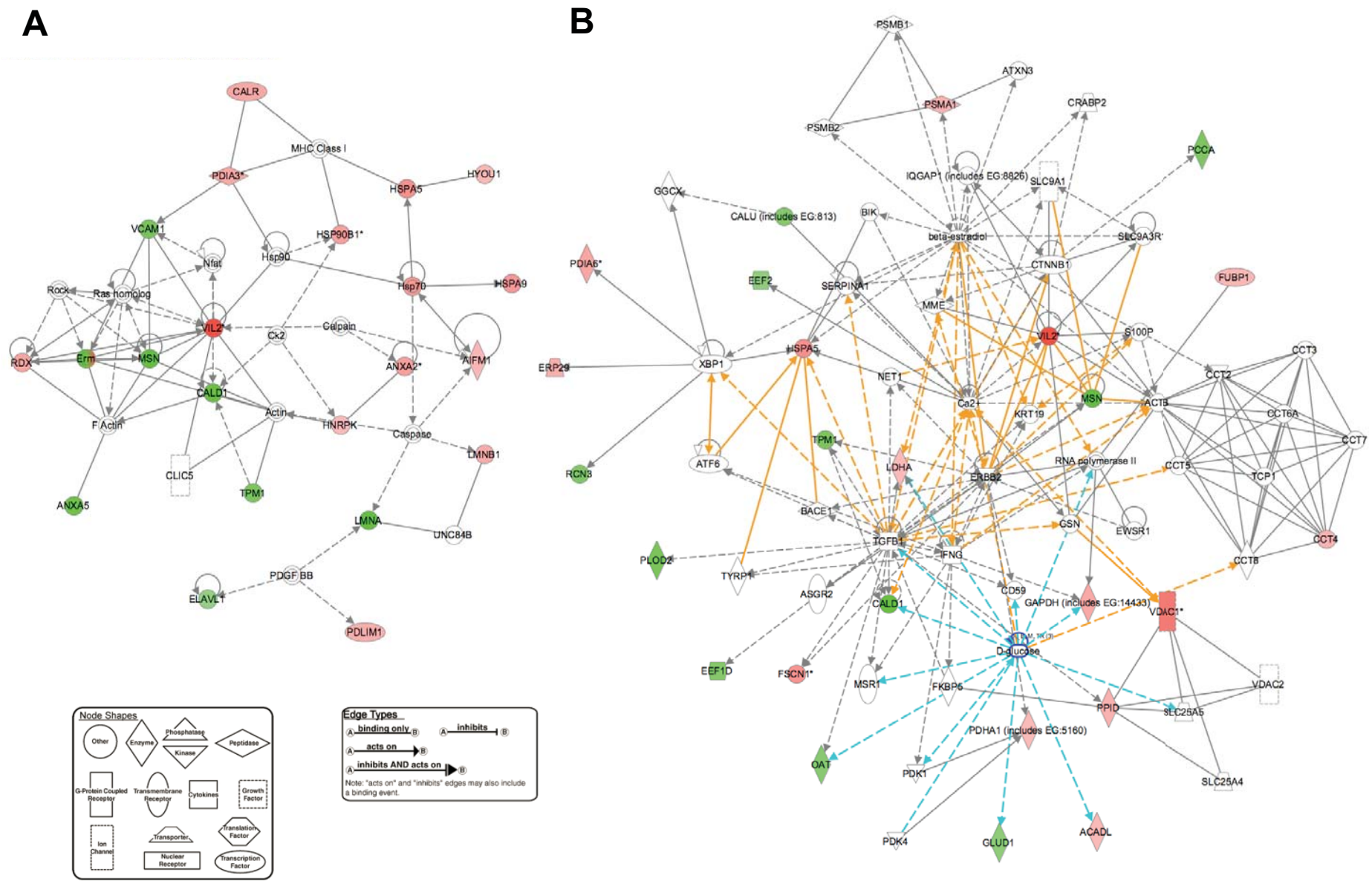

Supplemental Figure III **Mayr et al**

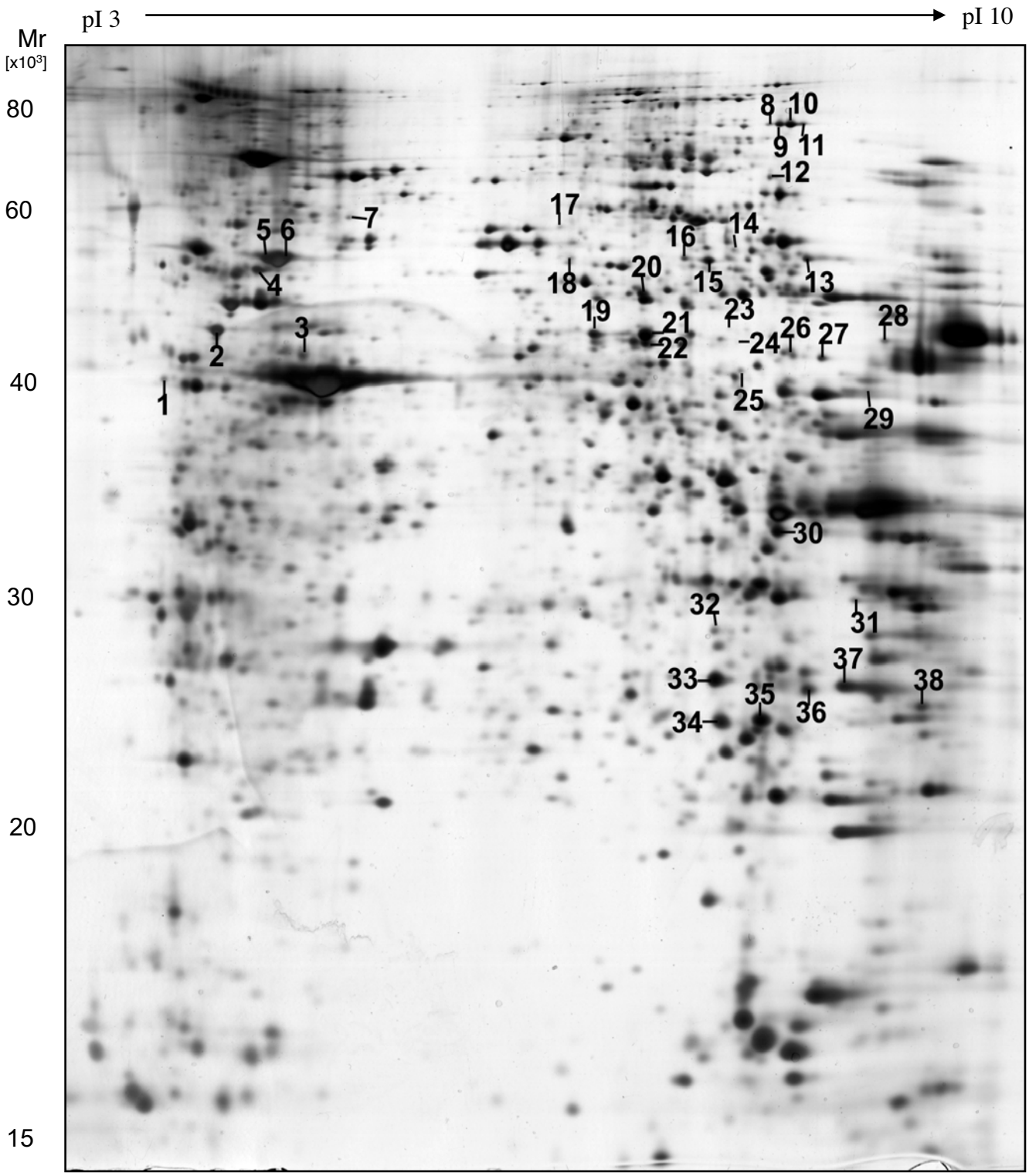

Supplemental Figure IV

Mayr et al

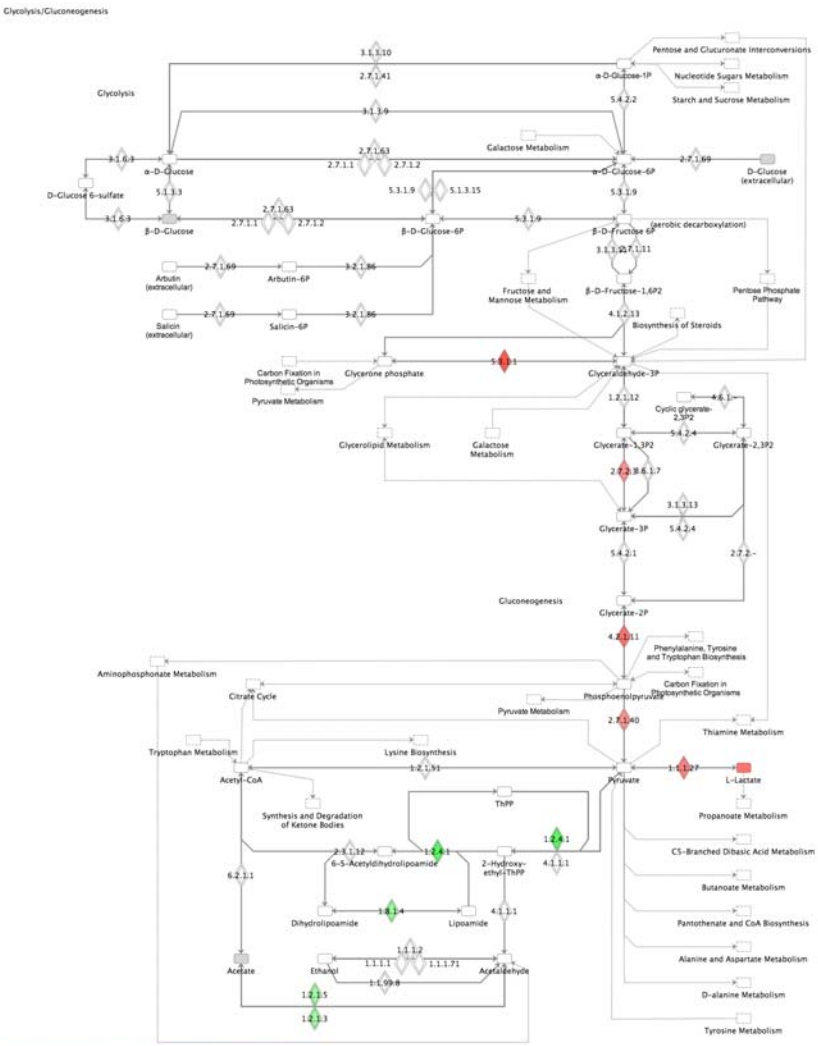

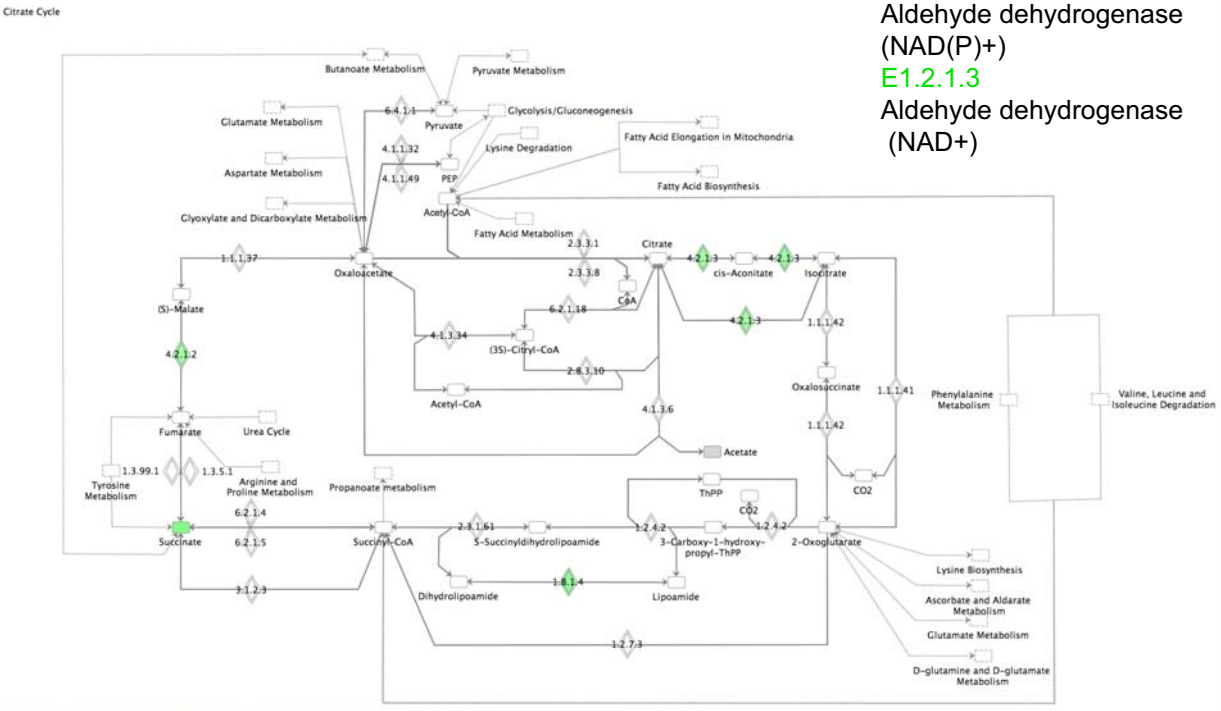

Node Shapes

Other Enzyme

GLYCOLYSIS:
E5.3.1.1
Triosephosphate isomerase
E2.7.2.3
Phosphoglycerate kinase
E4.2.1.11
Enolase
E2.7.1.40
Pyruvate kinase

PYRUVATE METABOLISM:
E1.1.1.27
L-lactate dehydrogenase

PDH COMPLEX:
E1.2.4.1
Pyruvate dehydrogenase
E1.8.1.4
Dihydrolipoamide dehydrogenase

TCA CYCLE:
E4.2.1.3
Aconitate hydratase
E4.2.1.2
Fumarate hydratase

LIPID METABOLISM:
E1.2.1.5
Aldehyde dehydrogenase (NAD(P)+)
E1.2.1.3
Aldehyde dehydrogenase (NAD+)

Supplemental Figure V **Mayr et al**

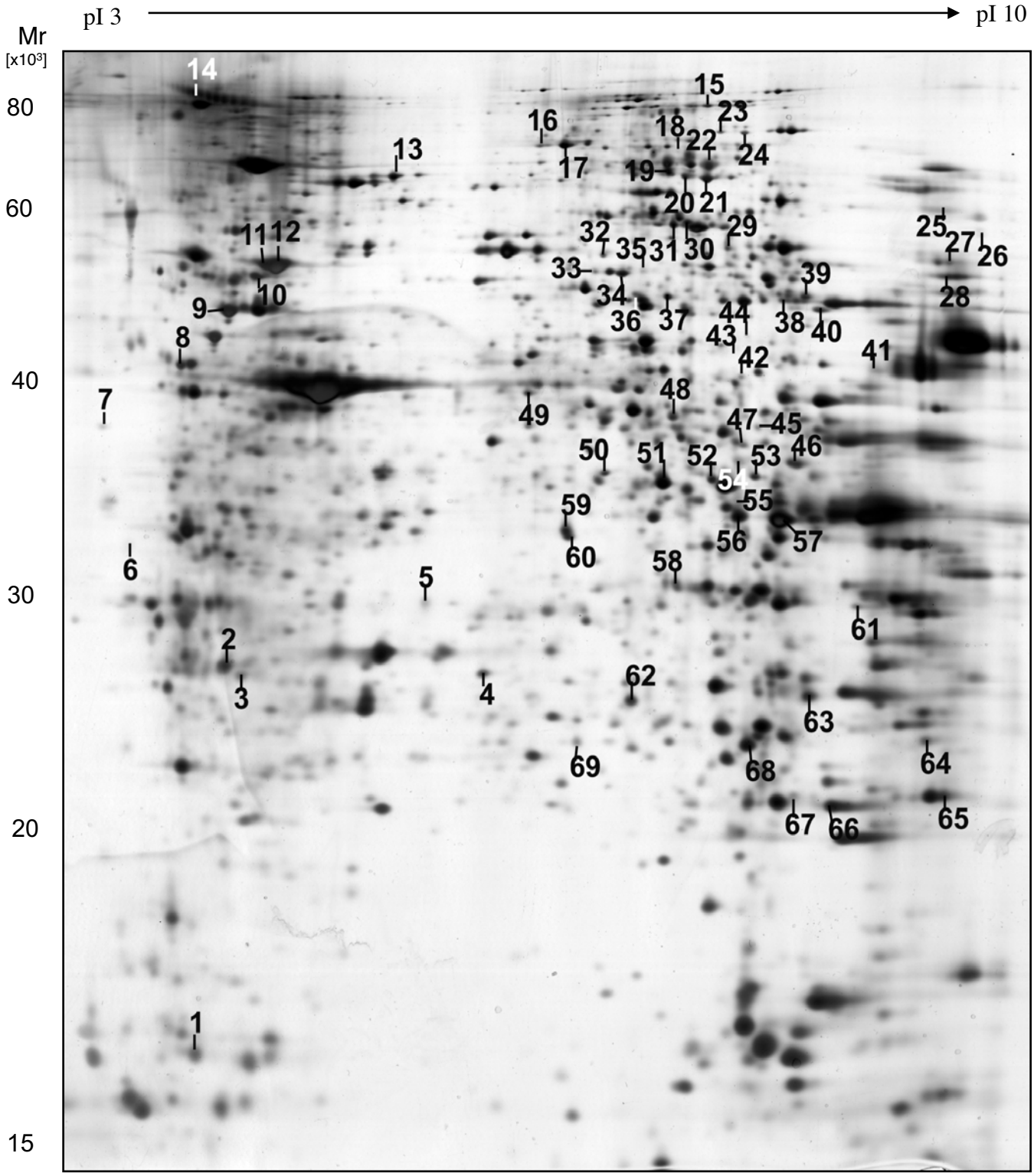

Supplemental Figure VI **Mayr et al**